SUPPLEMENTAL INFORMATION

Structure of a bacterial ribonuclease P holoenzyme in complex with tRNA

Nicholas J. Reiter[1], Amy Osterman[1], Alfredo Torres-Larios[1,2], Kerren K. Swinger[1,3], Tao Pan[4], and Alfonso Mondragón[1*]

[1]*Department of Molecular Biosciences, Northwestern University, Evanston, IL,60208 USA,*
[4]*Department of Biochemistry and Molecular Biology, University of Chicago, Chicago IL,60637 USA*

[2] Present address: Departamento de Bioquímica y Biología Estructural, Instituto de Fisiología Celular, Universidad Nacional Autónoma de México, Ciudad Universitaria, Apartado Postal 70-243, México 04510, México. [3] Present address: Abbott Laboratories, Abbott Park, IL 60064-6400, USA.

Holoenzyme	Substrate	Activity [k_{cat} / K_M (10^6 $M^{-1}min^{-1}$)]
RNase P, crystal P RNA*	crystal pre-tRNA (-1)*	5.9 ± 0.3
RNase P, crystal P RNA*	pre-tRNA (-9)	4.9 ± 1.0
RNase P, (w.t.) P RNA	crystal pre-tRNA (-1)*	14.0 ± 1.0
RNase P, (w.t.) P RNA	pre-tRNA (-9)	15.0 ± 3.0

Supplemental Table I. Enzymatic activity (k_{cat}/K_M) of the *T. maritima* RNase P and pre-tRNAs which gave crystals (as indicated by asterisks), and the "wild-type" *T. maritima* RNase P under single turnover kinetic conditions. Pre-tRNAs containing one (-1) and nine (-9) nucleotide leaders were tested.

Supplemental Table II: Data Collection

Crystal [a]	*NativeI*[b]	*NativeII*[b]	*Ta - I*	*Ta- II*	*Ta–III*	*Ir*	*Sm - I*	*Sm -II*	*Eu - I*	*Eu - II*	*Leader*	*Leader-Sm*
Energy (Å)	0.97872	0.97872	1.255653	1.25423	1.25186	1.1050782	1.601103	1.5497701	1.53713	1.546007	0.97872	0.97857
# of crystals	1	2	1	1	1	1	1	1	1	1	1	1
Resolution(Å)[c]												
Isotropic	30 - 3.80 (3.97-3.8)	30 - 3.80 (3.97-3.8)	30 - 4.65 (4.86 – 4.65)	30 - 4.6 (4.81 – 4.6)	30 - 4.75 (4.96 – 4.75)	30 - 4.1 (4.29 – 4.1)	30 - 4.55 (4.75 – 4.55)	30 - 4.40 4.60 – 4.40)	30 - 4.26 (4.45 – 4.26)	30 - 4.45 (4.65 – 4.45)	30 - 4.20 (4.80-4.20)	30 - 4.15 (4.33-4.15)
Anisotropic [c,d]	3.80 4.05 4.05 (3.97-3.8)	3.80 4.05 4.05 (3.97-3.8)	4.66 4.95 4.95 (4.86 – 4.66)	4.61 5.08 5.08 (4.82 – 4.61)	4.8 5.25 5.25 (4.98 – 4.77)	4.13 4.82 4.82 (4.31 – 4.13)	4.56 4.8 4.8 (4.76 – 4.56)	4.44 5.5 5.5 (4.64 – 4.44)	4.27 4.96 4.96 (4.46 - 4.27)	4.45 5.05 5.05 (4.66 – 4.45)	4.20 4.8 4.8 (4.39-4.20)	4.15 4.6 4.6 (4.35-4.15)
R_{meas} [e]	0.072(0.537)	0.100(0.530)	0.055 (0.446)	0.079 (0.532)	0.072 (0.494)	0.073 (0.568)	0.069 (0.470)	0.094 (0.582)	0.067 (0.559)	0.065 (0.543)	0.119(0.599)	0.089(0.590)
- anisotropic [d]	0.065(0.443)	0.096 (0.432)	0.053 (0.338)	0.070 (0.347)	0.067 (0.350)	0.062 (0.395)	0.065 (0.333)	0.076 (0.327)	0.059 (0.337)	0.058 (0.329)	0.099(0.577)	0.081(0.504)
$R_{merge.}$ [f]	0.063 (0.449)	0.082 (0.416)	0.045 (0.363)	0.072 (0.457)	0.059 (0.393)	0.061 (0.444)	0.061 (0.400)	0.079(0.461)	0.056 (0.443)	0.056 (0.444)	0.096 (0.478)	0.068 (0.454)
- anisotropic [d]	0.057 (0.389)	0.079 (0.359)	0.043 (0.295)	0.063 (0.306)	0.055 (0.300)	0.052 (0.305)	0.058 (0.299)	0.065(0.250)	0.050 (0.252)	0.051 (0.275)	0.081 (0.463)	0.061 (0.400)
Total # of Reflections	120377(10990)	143083(11629)	82473 (7864)	149166(11140)	75097 (7168)	127392(10995)	146013(13059)	111630(10485)	124664(11222)	130723(11867)	126530(11898)	102238(9543)
-anisotropic [d]	110767(3233)	135263 (3773)	76389 (2813)	125554 (2109)	65747 (1510)	99000 (816)	130117 (2820)	81874 (581)	99293(586)	109010 (1261)	103571(861)	87924(1184)
Unique Reflections	30324(3594)	30274 (3545)	16310 (1954)	16488 (1691)	15235 (1832)	24082 (2737)	17904 (2109)	19640 (2379)	21659 (2613)	19160 (2285)	22915(2757)	23565(2834)
-anisotropic [d]	26838(773)	27116 (842)	14465 (421)	13859 (278)	12550 (253)	17171 (218)	15203 (326)	13165 (167)	16094 (191)	14986 (225)	17674(231)	19252(343)
Completeness(%)[g]	86.3 (97.2)	98.8 (96.5)	98.8 (97.8)	97.7 (84)	98.9 (98.8)	98.7 (93.8)	99.1 (96.1)	99.4 (99.7)	99.3 (99.5)	99.6 (99.8)	99.5 (99.6)	98.3 (97.6)
- anisotropic [d]	87.4 (20.4)	88.5 (22.3)	87.7 (20.6)	83 (13)	82 (13.0)	71.0 (7.1)	84.6 (14.5)	67.8 (6.6)	73.5 (6.7)	77.9 (9.2)	76.4 (7.8)	80.8 (11.6)
Anom (%)[g,]	-	-	90.4 (79.8)	96.3 (79.7)	91.8 (84.0)	93.8 (83.5)	97.7 (91.7)	95.5 (91.2)	96.1 (91.1)	97.6 (94.0)	94.8 (90.0)	87.8 (77.5)
- anisotropic [d]	-	-	81.5 (19.1)	79.5 (11.8)	77.6 (11.5)	68.5 (6.1)	83.3 (13.4)	65.6 (5.2)	71.6 (5.3)	76.5 (8.1)	73.1 (6.1)	73.7 (9.3)
Mean <I>/σI [h]	11.9 (2.0)	11.0 (2.2)	15.4 (2.6)	14.8 (3.2)	11.4 (2.4)	12.4 (2.3)	16.1 (3.5)	10.9 (2.4)	13.3 (2.4)	14.7 (2.8)	8.7 (2.3)	9.6 (2.0)
- anisotropic [d]	13.2 (3.2)	12.2 (3.2)	16.9 (4.9)	16.8 (5.5)	13.3 (4.7)	15.6 (3.5)	18.5 (6.5)	14.9 (4.4)	17.0 (3.9)	18.0 (5.7)	10.7 (2.4)	11.4 (2.7)
Multiplicity [i]	4.0 (3.1)	4.8 (3.3)	5.1 (4.0)	9. 0(6.6)	4.9 (3.9)	5.3 (4.0)	8.2 (6.2)	5.7 (4.4)	5.8 (4.3)	6.8 (5.2)	5.5 (4.3)	4.3 (3.4)
- anisotropic [d]	4.1 (4.2)	5.0 (4.5)	5.3 (6.7)	9.1 (7.6)	5.2 (6.0)	5.8 (3.7)	8.6 (8.7)	6.2 (3.5)	6.2 (3.1)	7.3(5.6)	5.7 (3.7)	4.6 (3.5)
Anom Mult. [i]	-	-	2.8 (2.3)	4.6 (3.4)	2.7 (2.1)	2.8 (2.1)	4.2 (3.1)	3.0 (2.3)	3.0 (2.2)	3.5 (2.6)	2.9 (2.2)	2.4 (1.9)
- anisotropic [d]	-	-	2.9 (3.6)	4.8 (4.2)	2.8 (3.4)	3.0 (2.1)	4.4 (4.7)	3.3 (2.1)	3.3 (1.8)	3.8 (3.1)	3.1 (2.2)	2.5 (1.9)
MFID[j]	-	0.039	0.168	0.218	0.213	0.145	0.203	0.199	0.260	0.209	0.332	0.266

[a] Space group: $P3_121$, Unit cell parameters for native data sets: a=169.29; b=169.29; c=184.99; α=90; β=90; γ=120.
[b] *Native I* served as the reference dataset to determine experimental phases. *Native II* (*Native I* data merged with a second dataset) was used during refinement and served as the final native dataset.
[c] Numbers in parenthesis correspond to the highest resolution shell.
[d] Anisotropic Resolution is given for each direction (a, b, and c) of the crystal, respectively . Due to diffraction anisotropy observed in all data sets, poorly measured reflections in the a and b directions were excluded. The Diffraction Anisotropy Server[1] and an in-house script were implemented to exclude reflections beyond a prescribed resolution in each direction. Both methods gave identical results. The resolution (Å) in each direction (a, b, and c) and corresponding statistics are shown.
[e] R_{meas} as previously defined[2].
[f] $R_{merge} = \Sigma |I - \langle I \rangle| / \Sigma I$, where I = observed intensity, and <I> = average intensity obtained from multiple measurements.
[g] Percentage of completeness and anomalous completeness as defined by Scala[3].
[h] Mean I/ σI as defined by Scala[3].
[i] Multiplicity and anomalous multiplicity as defined by Scala[3].
[j] MFID (mean fractional isomorphous difference) = $\Sigma ||F1| - |F2|| / \Sigma |F1|$, where $|F1|$ = reference structure factor amplitude and $|F2|$ = compared structure factor amplitude.

Supplemental Table III: Phasing and Refinement

Crystal [a]	***Native I***	***Ta - I***	***Ta - II***	***Ta - III***	***Ir***	***Sm - I***	***Sm -II***	***Eu - I***	***Eu - II***
Energy (Å)	0.97872	1.255653 *Low remote*	1.25423 *Peak*	1.25186 *High remote*	1.1050782	1.601103	1.5497701	1.53713	1.546007
Phasing [b,c]	-		30.11 – 5.50[b]				29.6 – 4.1[c]		
Sites [b, c]	-	3	3	3	1	5	5	4	4
Phasing power [d]									
Dispersive (centric/accentric)	-	0.828/0.885	2.643/2.202	2.223/1.724	0.185/0.208	2.333/2.717	1.152/1.203	1.348/1.644	1.730/1.961
Anom. (accentric)		0.294	1.061	0.437	0.403	0.700	0.540	0.803	0.689
R-cullis factor									
Isomorphous		0.636	0.353	0.417	1.018	0.227	0.478	0.398	0.333
Anomalous		0.981	0.818	0.947	0.938	0.909	0.945	0.886	0.914
FOM (initial) (centric/accentric)	-		0.326/0.386				0.371/0.365		

Refinement [e]	TMCmplx anisotropic	TMCmplx isotropic	TMCmplx-Leader anisotropic
Resolution (Å) [f]	28.97 – 3.80 (3.94 – 3.80)	29.53 – 3.80 (3.93 – 3.80)	29.63 – 4.21 (4.46 – 4.21)
No. of reflections	27090	30251	17651
Test set [g]	1368	1541	913
R_{work} [h]	0.249 (0.248)	0.261 (0.311)	0.258 (0.236)
R_{free} [i]	0.270 (0.219)	0.281 (0.299)	0.267 (0.323)
No. of atoms	10113	10113	10144
r.m.s.d. Bond length (Å)	0.007	0.007	0.007
r.m.s.d. Bond angle (Å)	1.24	1.23	1.23
Ave. Wilson B [j]	129.78	131.82	153.42
Coord. Error(Å), DPI [k]	0.84	0.84	1.27

[a] Space group: $P3_121$, Unit cell parameters: a=169.29; b=169.29; c=184.99; α=90; β=90; γ=120.
[b] Initial experimental phases were determined to ~6.0 Å by Multi-wavelength anomalous dispersion (MAD) using only the Ta_6Br_{12} cluster derivative. Three Ta_6Br_{12} cluster locations were identified from the molecular replacement solution and subsequently verified in SHARP[4].
[c] Multiple Isomorphous Replacement with Anomalous Scattering (MIRAS) phases were determined to ~4.1 Angstroms using data from Ir, Sm, and Eu derivatives, and the output Hendrickson – Latham (HL) coefficients from the initial Ta_6Br_{12}-derived phases[4].
[d] Phasing power = r.m.s. ($|F\mathrm{h}|/E$) where $|F\mathrm{h}|$ = heavy atom structure factor amplitude and E = residual lack of closure error, reported for all acentric reflections.
[e] *Native II* data set was used for all refinement calculations performed in refmac5[5] and BUSTER[6]. Model refinement was performed using anisotropic and isotropic diffraction data from the *Native II* data set. TMCmplx refers to the *T. maritima* RNase P/tRNA complex. Model refinement of the *T. maritima* RNase P/tRNA complex with 5' leader sequence were calculated using the *Leader* experimental data set (Table SII).
[f] Numbers in parenthesis correspond represent all reflections in the highest resolution shell.
[g] R_{free} value test set (overall).
[h] $R_{work}=\Sigma||Fo|-|Fc||/\Sigma|Fo|$, where |Fo|=observed structure factor amplitude and |Fc|=calculated structure factor amplitude.
[i] R_{free} as defined by Brunger[7].
[j] Average Wilson B-factor generated from final refinement (reported in $Å^2$).
[k] The overall dispersion precision indicator (DPI) gives an estimated coordinate r.m.s. error for the final model (in Å).

Supplemental Table SIV Data collection and refinement statistics[a,b]

	Native II [c]	*TaBr I*	*TaBr II*	*TaBr III*	*Ir*	*Sm I*	*Eu I*	*Leader*	*Leader-Sm*
Data collection									
Space group	$P3_121$								
Cell dimensions									
a, *b*, *c* (Å)	169.3,	167.3,	167.1,	167.5,	169.5,	169.1,	169.6,	169.9,	170.9,
α, β, γ (°) =	169.3,	167.3,	167.1,	167.5,	169.5,	169.1,	169.6,	169.9,	170.9,
90°,90°,120°	185.0	184.3	183.5	183.3	184.5	184.8	184.1	185.5	185.7
		RemoteI	*Peak*	*RemoteII*					
Wavelength	0.97872	1.255653	1.25423	1.25186	1.10508	1.601103	1.53713	0.97872	0.97857
Resolution (Å)	30-3.8 (3.97-3.80)*	30 – 4.65 (4.86 - 4.65)	30 - 4.6 (4.81 - 4.6)	30 - 4.75 (4.96 - 4.75)	30 - 4.1 (4.29 - 4.1)	30 - 4.55 (4.75 - 4.55)	30 - 4.26 (4.45 – 4.26)	30 - 4.20 (4.39 – 4.20)	30 - 4.15 (4.35 – 4.15)
R_{meas}	0.10(0.53)	0.06(0.45)	0.08 (0.53)	0.07(0.49)	0.07 (0.57)	0.07 (0.47)	0.07(0.56)	0.12(0.59)	0.09(0.59)
R_{merge}	0.082 (0.416)	0.045 (0.363)	0.072(0.457)	0.059 (0.393)	0.061 (0.44)	0.061(0.40)	0.056(0.44)	0.096(0.48)	0.068(0.45)
$I/\sigma I$	11.0 (2.2)	15.4 (2.6)	14.8 (3.2)	11.4 (2.4)	12.4 (2.3)	16.1 (3.5)	13.3 (2.4)	8.7 (2.3)	9.6 (2.0)
Completeness (%)	98.8 (96.5)	98.8 (97.8)	97.7 (84.0)	98.9 (98.8)	98.7 (93.8)	99.1 (96.1)	99.3 (99.5)	99.5 (99.6)	98.3 (97.6)
Redundancy	4.8(3.3)	5.1 (4.0)	9. 0(6.6)	4.9 (3.9)	5.3 (4.0)	8.2 (6.2)	5.8 (4.3)	5.5 (4.3)	4.3 (3.4)
Refinement	TMCmplx (anisotropic)	TMCmplx (isotropic)						TMCmplx-Leader	
Resolution (Å)	28.97-3.8 (3.94-3.8)	29.53-3.8 (3.93-3.8)						29.63-4.21 (4.46-4.21)	
No. reflections	27090	30251						17651	
Test set	1368	1541						913	
$R_{work/}$ R_{free}	0.249/0.270 (0.248/0.219)	0.256/0.281 (0.311/0.300)						0.258/0.267 (0.231/0.323)	
No. atoms	10113	10113						10144	
Protein	973	973						973	
Nucleic Acid	9126	9126						9166	
Ligand/ion	14	14						5	
Ave. B-factors	129.78	131.82						153.42	
R.m.s deviations									
Bond lengths (Å)	0.007	0.007						0.007	
Bond angles (°)	1.24	1.23						1.23	

[a] All data collection, phasing, and refinement statistics can be found in supplemental tables I-III.
[b] Standard isotropic diffraction is given as data collection statistics.
[c] Two datasets (Native II) serve as the reference dataset for experimental phases.
*Highest resolution shell is shown in parenthesis.

M1	
G1 O1P	2.0
U52 O4	2.1
A50 O1P	2.1
A50 O3′	2.4
A50 O2P	2.7
G1 O3P	2.9
A50 O5′	3.4
G51 O2P	3.5
G1 O5′	3.5
A49 O3′	4.1

M2	
G51 O2P	2.2
G51 O1P	3.0
G1 O3′	3.3
G1 O3P	3.8
G1 O1P	4.1

Supplemental Table V. Ligand distances to potential catalytic metal ions (M1 and M2) in the RNase P active site. All potential metal ligands (≤ 4.1 Å) are shown, and include P RNA (black), tRNA (red), and leader (purple) molecules.

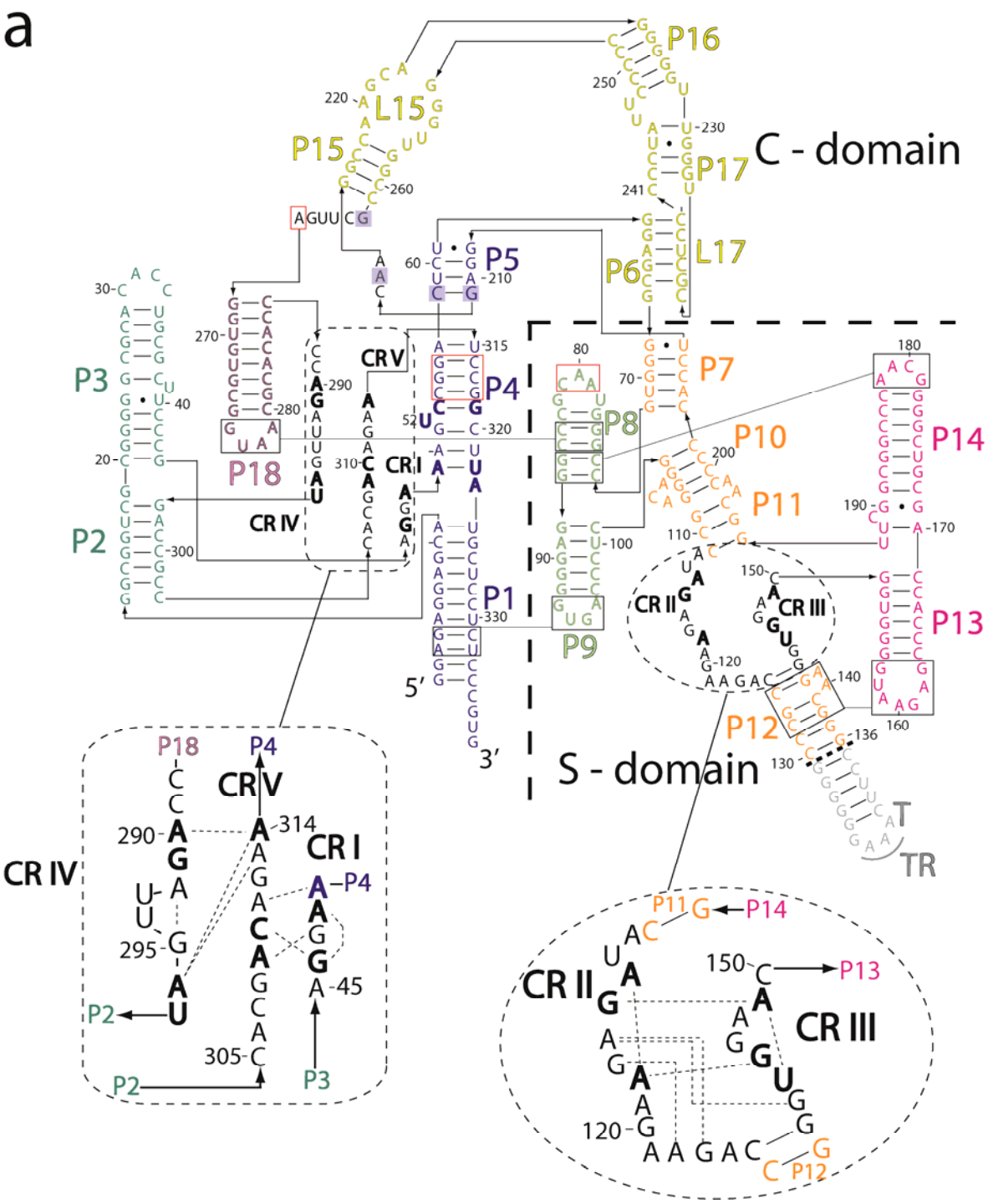
a
P16
L15
P15
P17
C - domain
P5
P6
L17
P3
P4
P7
P8
P10
P14
P18
CR V
CR I
P11
P2
CR IV
P1
P9
CR II
CR III
P13
5′
3′
S - domain
P12
T
TR
P18
P4
CR V
CR IV
CR I
P2
P3
P11
P14
CR II
CR III
P13
P12

b

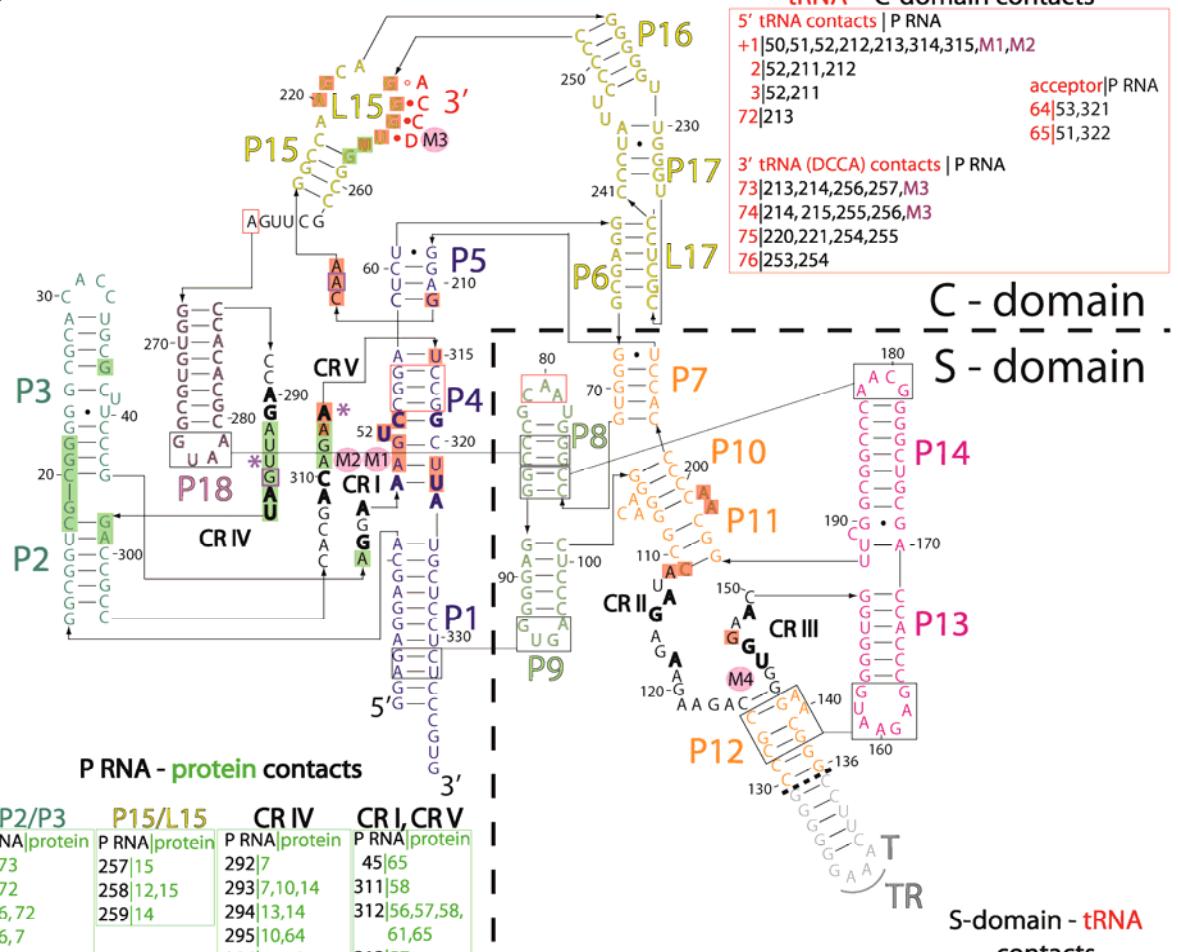

tRNA - C-domain contacts

5′ tRNA contacts | P RNA
+1|50,51,52,212,213,314,315,M1,M2
2|52,211,212
3|52,211
72|213

acceptor|P RNA
64|53,321
65|51,322

3′ tRNA (DCCA) contacts | P RNA
73|213,214,256,257,M3
74|214, 215,255,256,M3
75|220,221,254,255
76|253,254

P RNA - protein contacts

P2/P3	
P RNA	protein
18	73
19	72
20	6, 72
21	6, 7
22	7
37	8
298	62, 65, 66, 69, 73
299	62,66, 73

P15/L15	
P RNA	protein
257	15
258	12,15
259	14

CR IV	
P RNA	protein
292	7
293	7,10,14
294	13,14
295	10,64
296	64,68
297	65,68

CR I, CR V	
P RNA	protein
45	65
311	58
312	56,57,58, 61,65
313	57

5′ leader contacts

Protein - 5′ leader		P RNA - 5′ leader		tRNA - 5′ leader	
R52, R56	-1 backbone	A314	-1*	+1	-1
F17	-3	G295	-1, -2	metal - 5′ leader	
F17,F21,K51	-4	A213	-1, -2*	M2	-1
K51,P88, R89, K90	-5	U294	-3*		

S-domain - tRNA contacts

P RNA | tRNA	
111|19, 56	TΨC & D loops
112|19,56	
147|56	
195|56	
196|55	T stem
197|54	
198|53,54,61,62	
199|58,61	

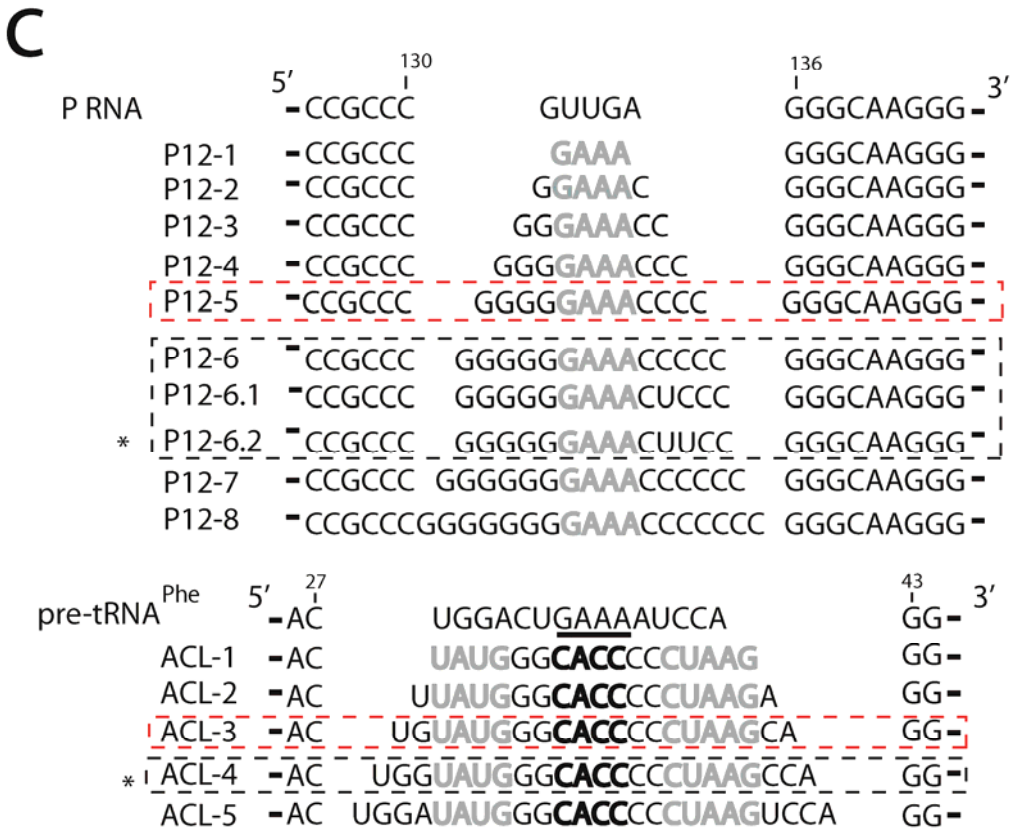

Figure S1 | Schematic diagram of *T. maritima* P RNA. a, Sequence and secondary structure of P RNA showing major intramolecular interactions observed in the crystal of the RNase P holoenzyme/tRNA complex. Filled circles represent non-canonical base pairing; arrows indicate 5′ to 3′ direction; and lines linking boxed nucleotides represent tertiary interactions. Boxed nucleotides in red represent a tertiary A-minor interaction between the essential P4 core, the P8 loop, and also includes a previously unrecognized nucleotide A267 at J15/18 which participates in the A-minor stack. All other tertiary interactions are shown by black boxes connected by a line. Bold nucleotides denote positions that are universally conserved, and these nucleotides are located in five different conserved regions (CR) of the P RNA (bold, black). Nucleotides shaded in blue represent positions that are conserved in all bacteria. The CR regions in the S-domain and C-domain are expanded to show interactions (dashed lines) that occur within the conserved nucleotide regions. A thick, dashed line between residues 130 and 136 distinguishes the *T. maritima* P RNA sequence from the engineered tetraloop (T)-

tetraloop receptor (TR) RNA module (light grey). P RNA nomenclature and coloring is the same as Figure 2, where the coaxial P1/P4/P5 stem is shown in blue, P2/P3 stems in cyan, P6/P15/P16 and L15/L17 in yellow, P7 and P10/P11/P12 in orange, P8/P9 in light green, and P13/P14 in pink. **b,** Secondary structure of P RNA mapping the major intermolecular interactions observed between P RNA and tRNA (red) and the P RNA and protein (green). P RNA nomenclature and coloring is the same as in A. Nucleotides shaded in pink make contacts with the tRNA, and boxed nucleotides shaded in green make contacts with the protein. Pre-tRNA 5′ leader interactions are noted with an asterisk (purple) and represent potential contacts if nucleobase and ribose moieties are appended to the structure of the 5′ leader. P RNA nucleotides that contact both tRNA and protein are shaded in pink with green borders. P RNA nucleotides that contact the 5' leader contain purple boxes. Tables of the P RNA – tRNA intermolecular contacts are shown, and categorized into specific regions. Tables of the P RNA – protein and RNase P – 5′ leader intermolecular contacts are also shown. All identified RNase P – tRNA contacts are within 4 Å. All identified RNase P - 5' leader contacts are within 4.5 Å. **c,** Regions of the P RNA sequence (top) at the P12 helix (P12) are replaced with the tetraloop (bold grey) and have increasing base pairs. The anticodon loop (ACL) of tRNA (bottom) was also changed to enable tetraloop recognition (bold grey) with P RNA and contains an altered tetraloop (bold black) to replace the natural GAAA sequence present in this $tRNA^{Phe}$ and that could serve as a GNRA tetraloop. Forty-two combinations were tested. Dotted boxes are paired combinations which yielded crystals (black and red), and an asterisk denotes the paired combination which gave diffraction to 3.8 Å.

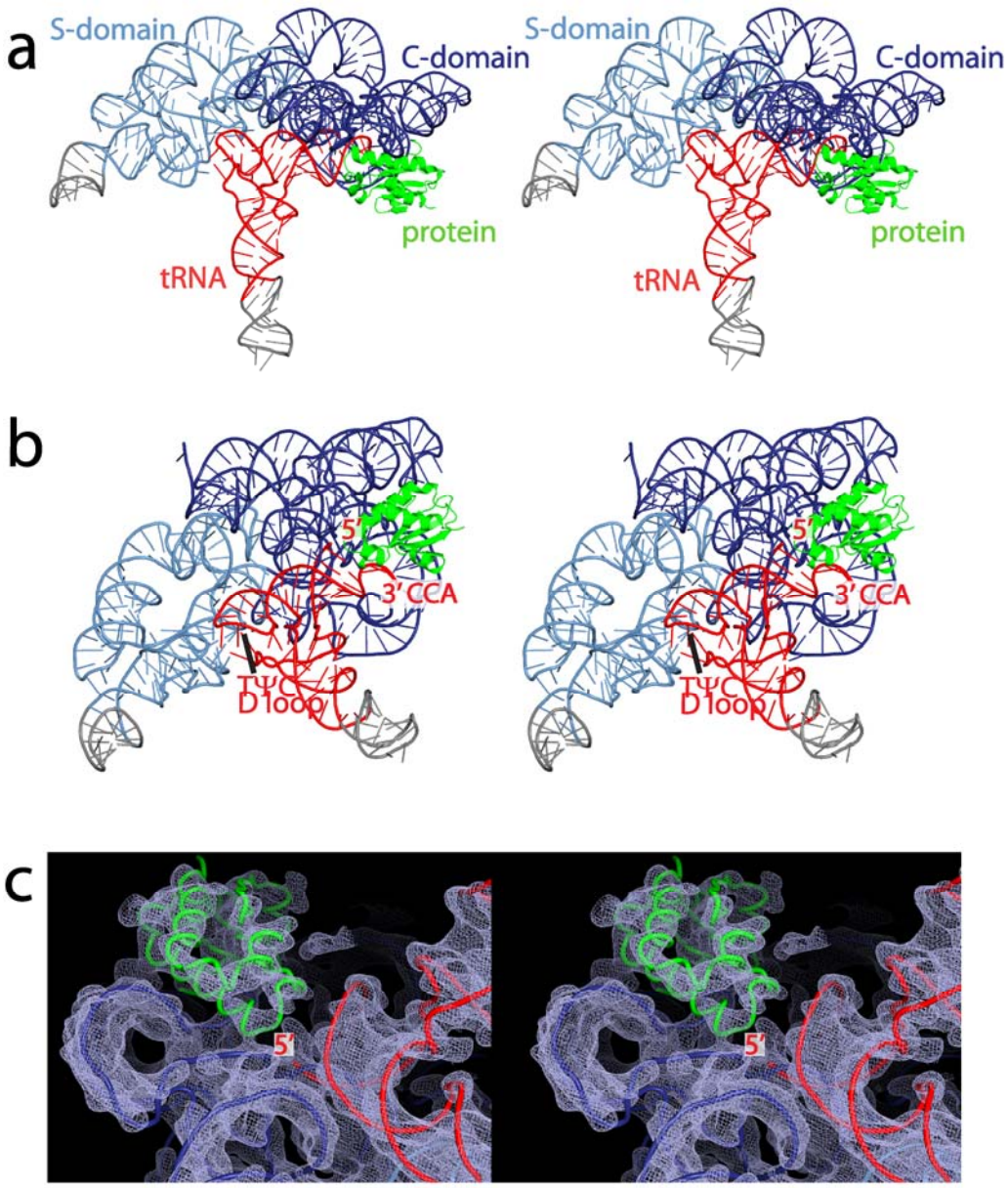

Figure S2 | Stereo diagram of the *T. maritima* RNase P holoenzyme in complex with tRNA. Supplemental to Figure 1. a, Stereo diagram of the overall structure of a bacterial RNase P-tRNA (enzyme-product) complex. **b,** Alternate stereo view of the RNase P-tRNA complex, emphasizing the P RNA-tRNA interactions **c,** The unbiased, solvent-flattened, experimental electron density map is represented as a blue-white mesh, contoured at 1.4 rmsd. The picture is centered on the 5′ end of tRNA. The P RNA (blue), tRNA (red), and protein (green) backbones traces are shown. The color scheme is identical to the one in Figure 1.

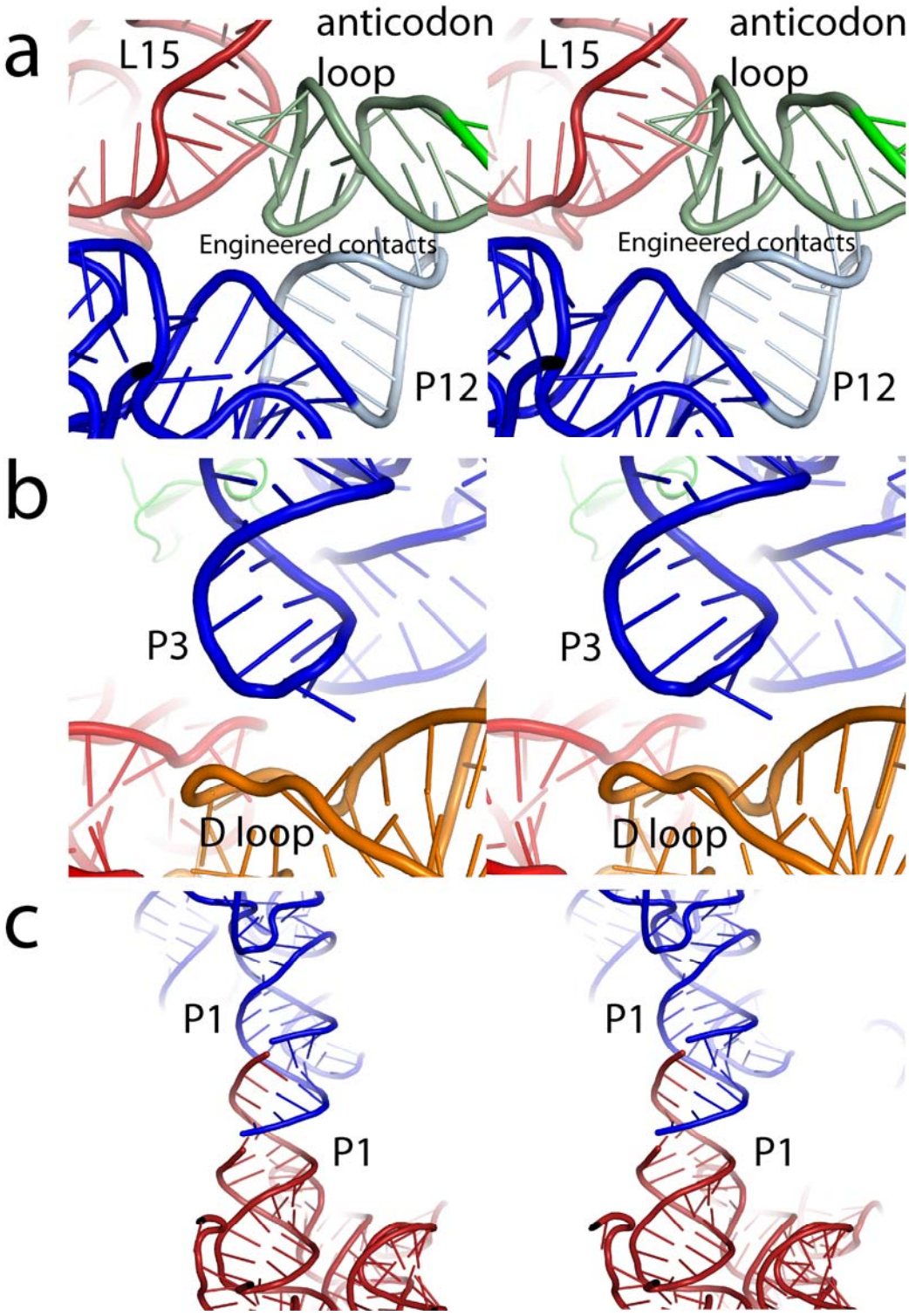

Figure S3 | Lattice contacts in the crystals of the *T. maritima* RNase P holenzyme and tRNA. a, Engineered crystal contacts between the P12 stem of P RNA and the anticodon loop of tRNA. A tetraloop-tetraloop receptor was introduced to favor crystal lattice formation. The tetraloop was placed in the loop capping the P12 stem and the tetraloop receptor was placed in the anticodon stem of tRNA. In

addition to the tetraloop/tetraloop receptor interactions, the loop capping the anticodon stem interacts with one nucleotide of the L15 loop in a neighboring molecule. The P12 stem is shown in blue with the engineered tetraloop receptor in light blue, the anticodon stem is shown in green with the tetraloop receptor in light green, the neighboring L15 loop is shown in red. **b,** Crystal contact between the P3 helix and the D loop of tRNA. The P3 stem is shown in blue and tRNA from a neighboring molecule in orange. **c,** Crystal contact between two symmetry-related P1 stems. The unpaired regions at the 3′ end of the molecule come together to form a continuation of the P1 stem.

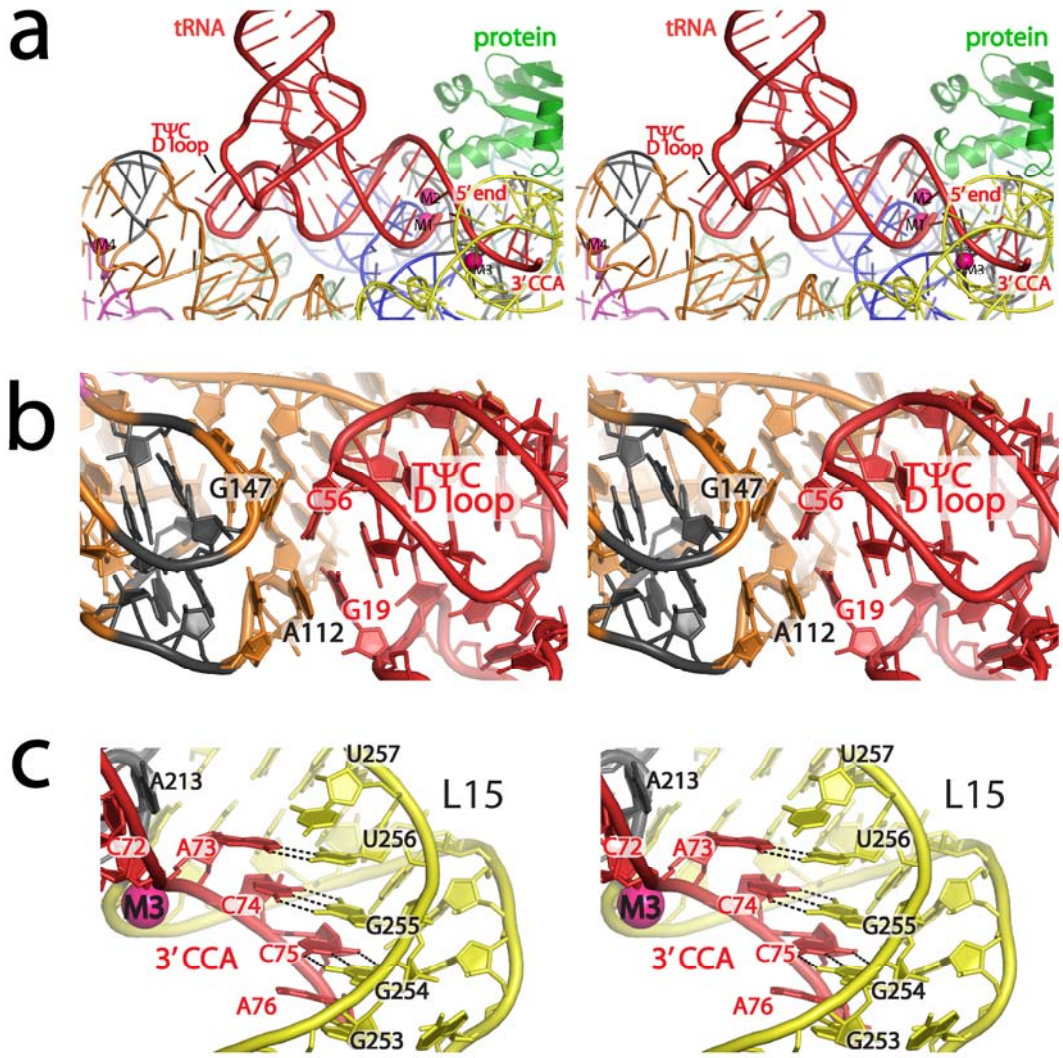

Figure S4 | Stereo diagrams showing tRNA recognition by the P RNA of RNase P. Supplemental to Figure 2. a, Stereo diagram illustrating overall tRNA recognition by the P RNA of RNase P. **b,** Stereo diagram illustrating tRNA recognition by the S-domain. Note that in free tRNA, the TΨC loop caps the acceptor stem and also interacts with the D loop *via* an intercalated base. In the case of the S-domain, the unstacking of the interacting bases is a consequence of two intertwined T loop motifs[8], which form two universally conserved regions (CR-II and CR-III). **c,** Intermolecular base pairing of the tRNA 3′ end (ACC) and the L15 (GGU) loop of P RNA. Labels and color scheme as described in Figure 2.

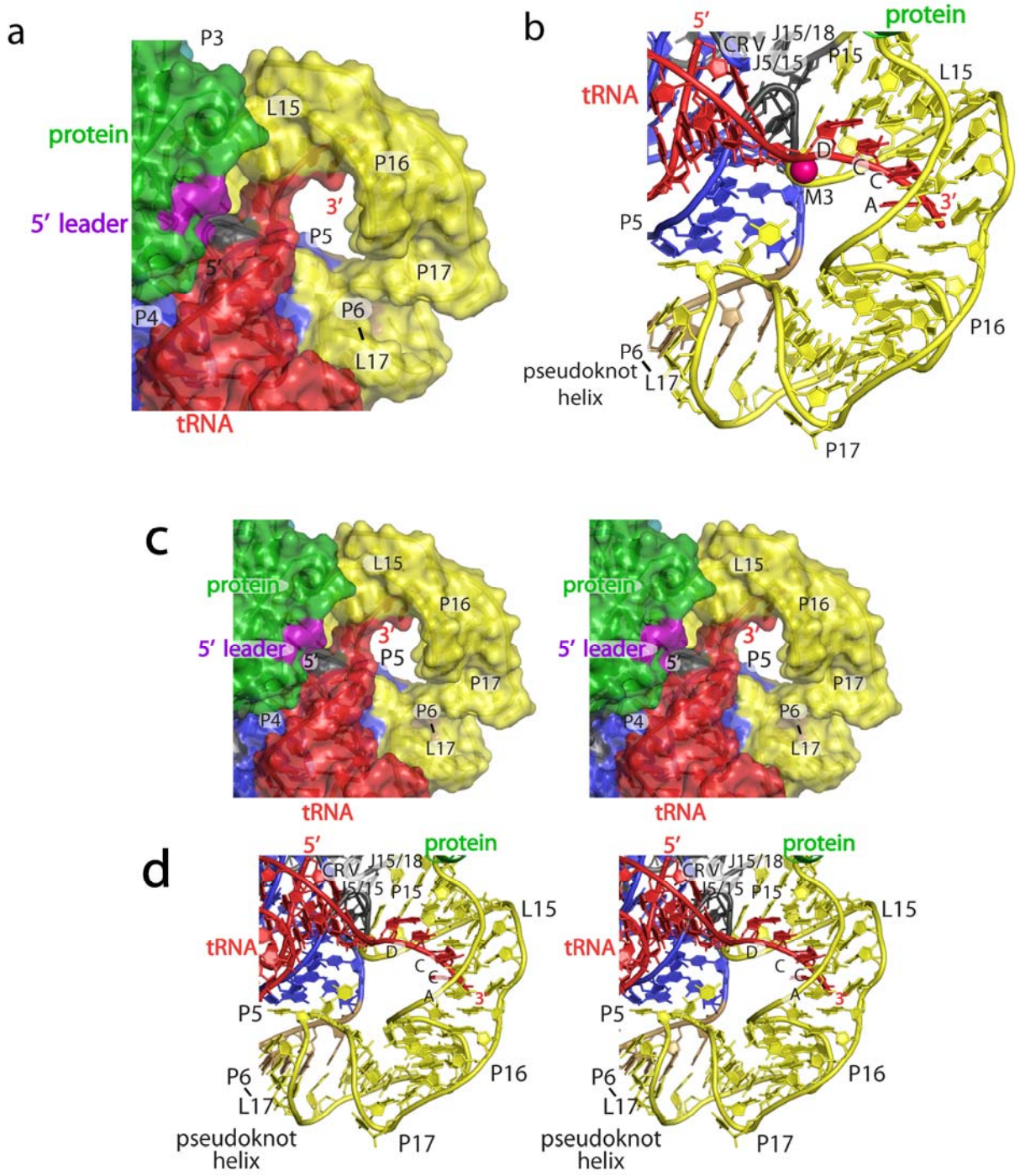

Figure S5 | Intermolecular base pairs at the 3′ CCA region of tRNA. a, Surface representation emphasizing the large diameter (18-25 Å) tunnel that accommodates the 3′ end of tRNA (red). This interaction is facilitated by the pseudoknot structure (yellow), which contains three helices (P15,16,17) and two important loop regions, L15 and L17, that base pair with the 3′ end of tRNA and the P6 region (light brown), respectively. This region almost completely encloses the 3′ end of the tRNA, suggesting that the creation of the tunnel could be triggered by the formation of the

intramolecular P6/L17 pseudoknot helix concomitant with tRNA recognition. Other regions surrounding the 3′ CCA motif include: protein (green), 5′ leader (purple), P3 (cyan) and P4/P5 helices (blue) of the P RNA, and the conserved CRV, J5/15, and J15/18 regions (grey). **b,** Three canonical intermolecular base pairs form between the nucleotides at the 3′ end of tRNA (A(D), C, C) and nucleotides in the L15 loop (G, G, U) of P RNA. A fourth intermolecular base pair (A76 – G253) may also occur but is ambiguous in the structure. The tRNA-P RNA interaction is stabilized by a metal ion (M3, magenta sphere), and a L15 ribose zipper conformation. In addition to recognition, the 3′ end of tRNA and L15 region of P RNA may participate in the mechanism of product release[9,10]. The discriminator base of tRNA and the protein component play known roles in modulating the rate of product release under multiple turnover conditions[9,11-13]. Intriguingly, the structure of the complex reveals that the discriminator tRNA–P RNA base pair (A73-U256) is uniquely positioned adjacent to a conserved arginine rich region of the protein (Arg 12,14, and 15) that makes contacts with P RNA residues U257 and G258. Further structural and mechanistic experiments will be required to decipher the mechanism of product release. Panels **c** and **d** represent stereo diagrams of figures S5a and S5b, respectively.

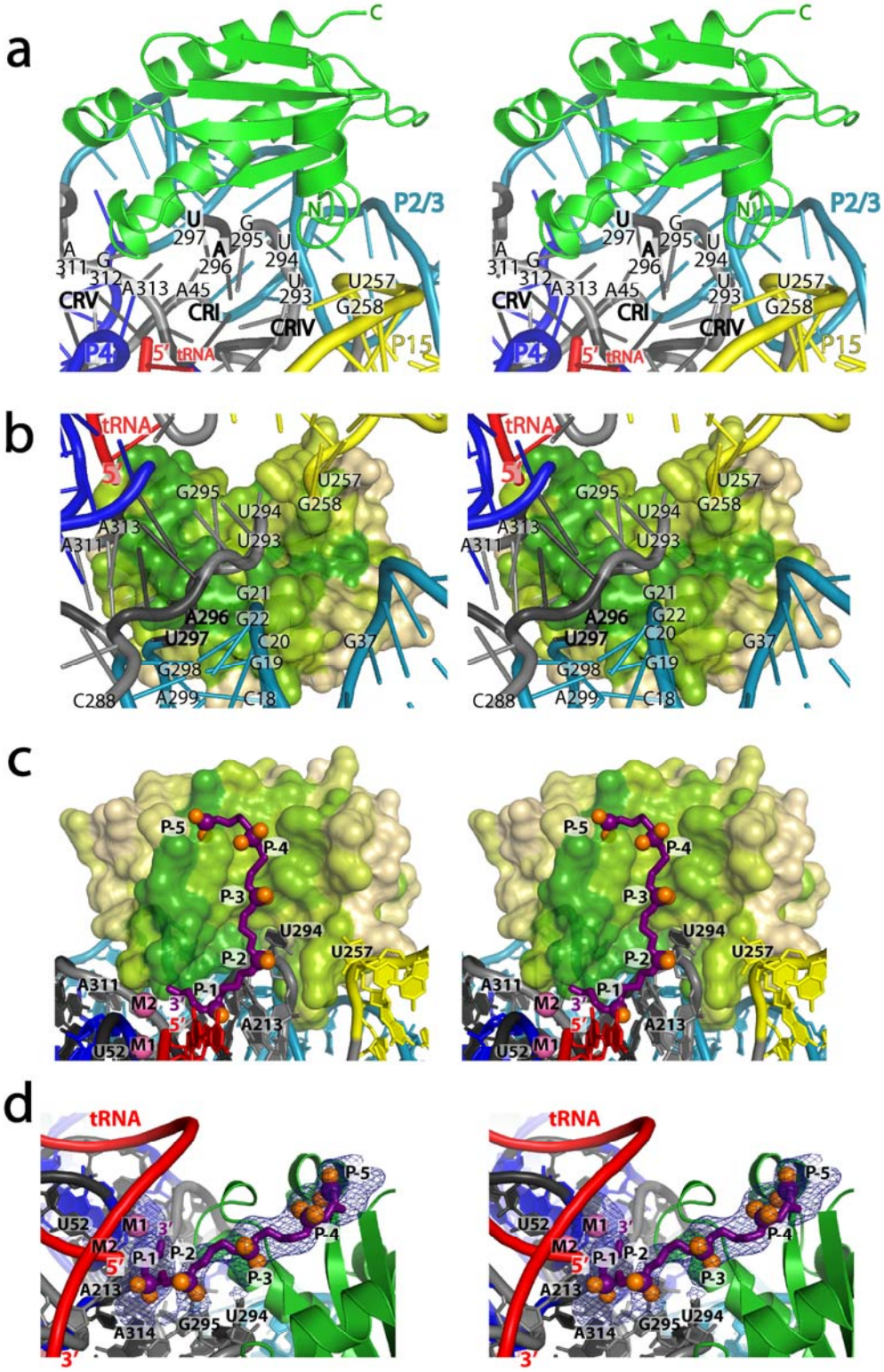
a
C
P2/3
U
297
G
295
U
294
A
296
A
311
G
312
A313
A45
U
293
U257
G258
CRV
CRI
CRIV
P4
5′ tRNA
P15
b
tRNA
5′
G295
U257
U294
G258
A313
A311
U293
G21
A296
G22
U297
C20
G37
G19
G298
C288
A299
C18
c
P-5
P-4
P-3
U294
U257
P-2
A311
P-1
M2
3′
5′
A213
U52
M1
d
tRNA
P-5
U52
M1
3′
P-4
M2
5′
P-1
P-2
P-3
A213
A314
G295
U294
3′

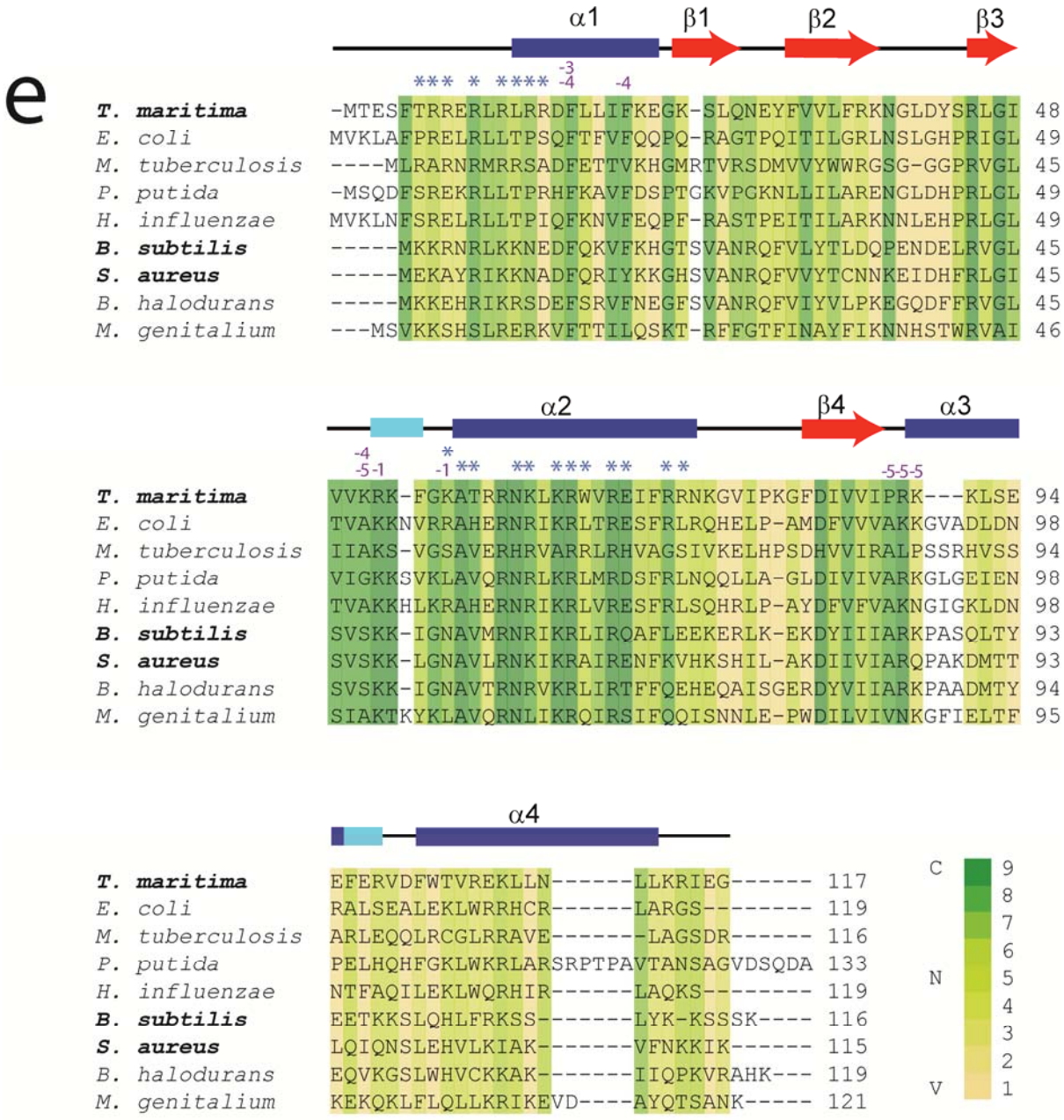

Figure S6 | Protein-RNA contacts within the RNase P holoenzyme. Supplemental to Figures 3 and 4. a, Stereo diagram emphasizing contacts between the protein and the P RNA (as colored in Fig. 2 and defined in Fig. 3). Specific P RNA/P protein contacts between the base of the P15 helix and conserved protein residues (Arg12, Arg14, and Arg15) may help stabilize the P15/P16/P17/P6 region. The opening is not found in B-type RNase Ps, which contains the L15 loop without the pseudoknot[14,15]. **b,** Stereo diagram of the surface representation of the protein colored by sequence conservation and emphasizing contacts with the P RNA. Note that there are no direct contacts between the protein

and mature tRNA. **c,** Stereo diagram of the surface of the protein colored by sequence conservation. The leader follows a highly conserved patch in the protein extending from the 5′ end of the mature tRNA (red) and away from the P RNA. **d,** Alternative stereo diagram of the pre-tRNA leader/protein interactions. **e,** Sequence alignment of the RNase P protein component from several bacteria**.** The first five sequences correspond to A-type molecules and the bottom four sequences correspond to B-type molecules. Names in bold denote proteins whose structure is known. A blue asterisk above an amino acid denotes a contact (≤ ~4 Å) with the P RNA, while a purple number indicates a contact with the -1, -2, -4, and -5 phosphate in the 5' pre-tRNA leader (≤ ~4.5 Å). Secondary structure elements are shown on top (red: beta strands, blue: alpha helices, cyan: 3_{10} helices). Nomenclature according to Kazantsev *et al.* [16]. A-type sequences: *T. maritima (*gi:9789801), *E. coli* (gi:290552), *M. tuberculosis* (gi: 61234238), *P. putida* (gi:60393731), and *H. influenzae* (gi: 42631319). B-type sequences: *B. subtilis* (gi: 585905), *S. aureus* (gi: 296275688), *B. halodurans* (gi: 15616627), and *M. genitalium* (gi: 255660032). In panels **b**, **c**, and **e**, the sequences are colored by sequence conservation on a scale of 1 to 9 (1:Variable: tan, Neutral: light green, 9:Conserved: green). Four hundred and ninety bacterial RNase P proteins were included in the analysis of sequence conservation using the ConSurf server[17].

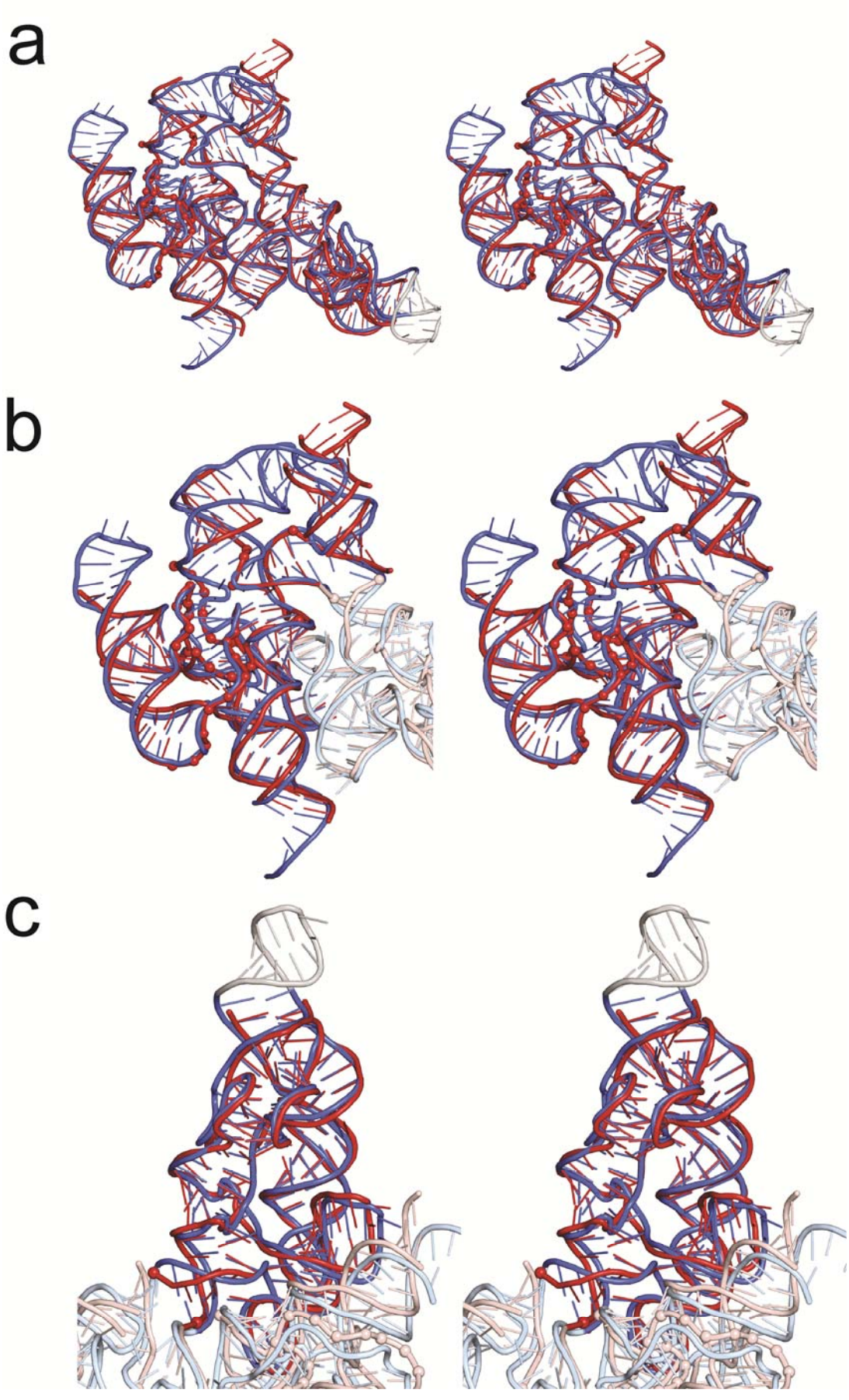
a
b
c

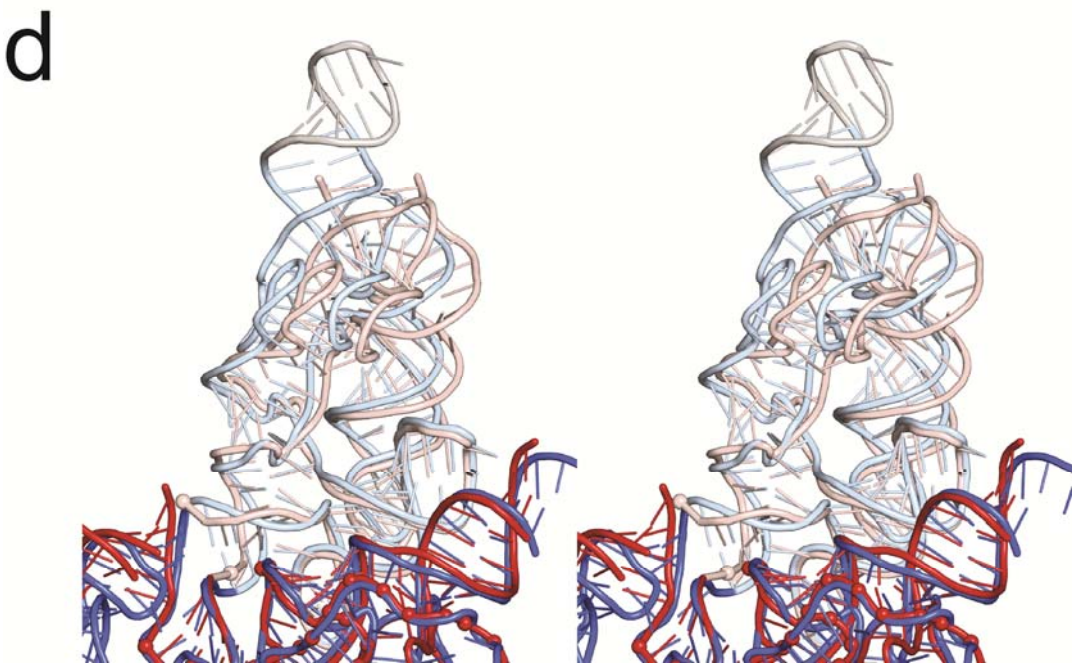

Figure S7 | Superposition of free P RNA and P RNA in the holenzyme/tRNA complex. a, Stereo diagram showing the superposition of the entire P RNA found in the free molecule (red) and in the holoenzyme/tRNA complex (blue). The normalized rms deviation for the sugar phosphate backbone is 1.1 Å. There are no large structural changes that could be attributed to the presence of the protein, suggesting that the protein plays a minor role in P RNA stabilization. Furthermore, the sequence conservation observed in some of the universally conserved regions cannot solely be attributed to interactions with conserved regions in the protein, as the protein itself is not conserved in higher organisms. **b,** Stereo diagram of the C-domains after superposition of the C-domains for the P RNA in the free molecule (red) and holoenzyme/tRNA complex (blue). Nucleotides in the S-domains are shown in pink and light blue for the free and complex structures, respectively. The normalized rms deviation for the sugar phosphate backbone in the C-domains is 2.2 Å. **c,** Stereo diagram of the S-domains after the superposition of the S-domains for the P RNA in the free (red) and holoenzyme/tRNA (blue) complex. Nucleotides in the C-domains are shown in light pink and light blue for the free and complex structures, respectively. The normalized rms deviation for the sugar phosphate backbone in the S-domains is 0.8 Å. **d,** Stereo diagram showing the S-domain after superposition of the C-domains for the P RNA in the free (red) and holoenzyme/tRNA (blue) complex. The comparison shows a small change (~7.5°) in

the relative orientation of the S- and C- domains, which may indicate the need for some plasticity in the ribozyme to accommodate slightly different substrates. Nucleotides in the S-domains are shown in pink and light blue for the free and complex structures, respectively. The diagram illustrates the relative movement of the two domains. In all diagrams, the additional nucleotides added to promote crystal formation are shown in grey. Superpositions were done with the program lsqman[18].

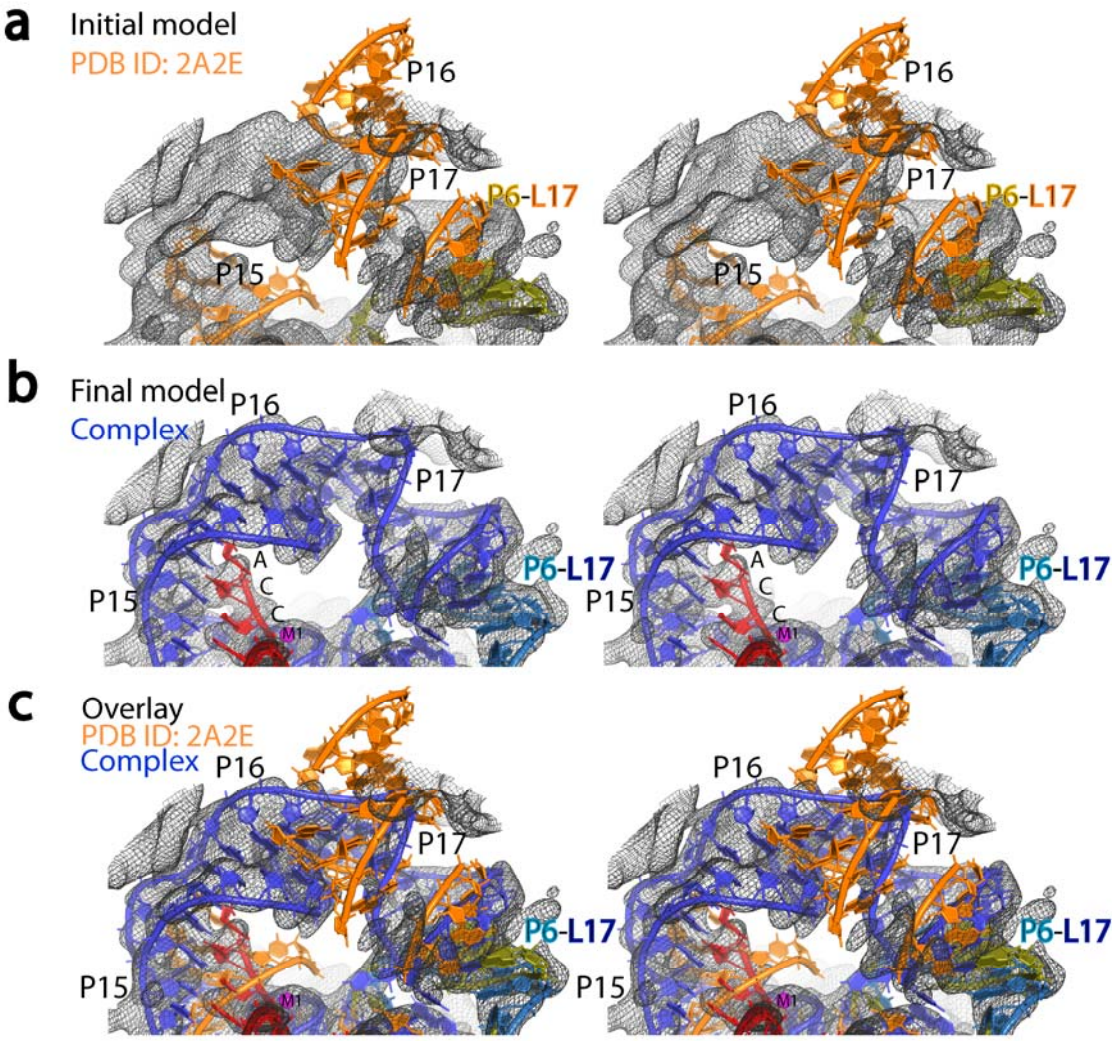

Figure S8 | The P15-P17 region of P RNA was completely rebuilt using only the experimental map as a guide. While most regions of the P RNA were fit into the experimental map using known structures[15,19] as a guide, the P15-P17 region adopts a completely different fold from the one observed in the free P RNA structure and was built using only the experimental map as a guide. This region of bacterial RNase P is unique as it adopts a non-A-form helical structure, contains the only intermolecular base pairs with tRNA, folds into a ribose zipper structure, and forms an intramolecular pseudoknot helix. **a**, Stereo diagram showing the *T. maritima* P RNA apo-structure (PDB 2A2E)[19] and the experimental map (1.5 rmsd contour level, black mesh). **b**, Stereo diagram showing the final structure of the complex (blue) and the experimental map (1.5 rmsd level, black mesh). **c**, Stereo diagram showing a superposition of the apo-P RNA and complex structures and the experimental map (1.5 rmsd contour level, black mesh). The superposition

emphasizes the large structural differences between the P RNA apo-structure (PDB 2A2E) and the structure of the RNase P holoenzyme-tRNA complex. In all panels, empty map regions correspond to electron density from symmetry related molecules.

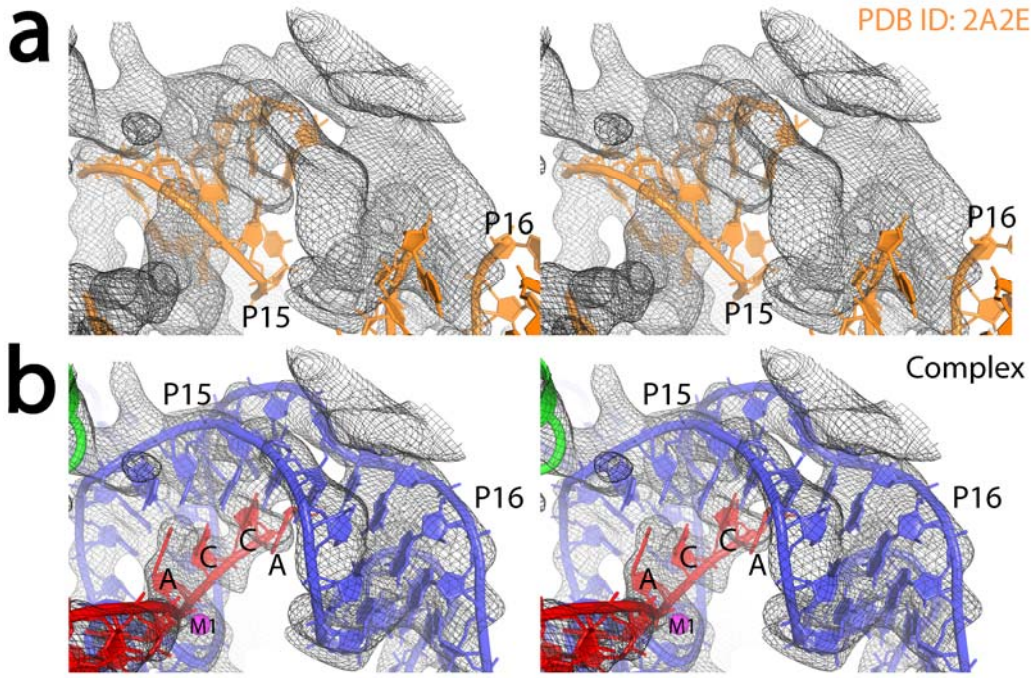

Figure S9 | The P15/P16 helices and the P RNA-tRNA intermolecular base pair region. a, Stereo diagram of an alternative view of Figure S8a, illustrating the differences between the experimental map (1.5 rmsd contour level, black mesh) and the P RNA apo-structure (2A2E)[19]. **b**, Stereo diagram of the final model of the complex (blue) and the experimental map (1.5 rmsd contour level, black mesh). As in Figure S8, empty map regions correspond to electron density from symmetry related molecules.

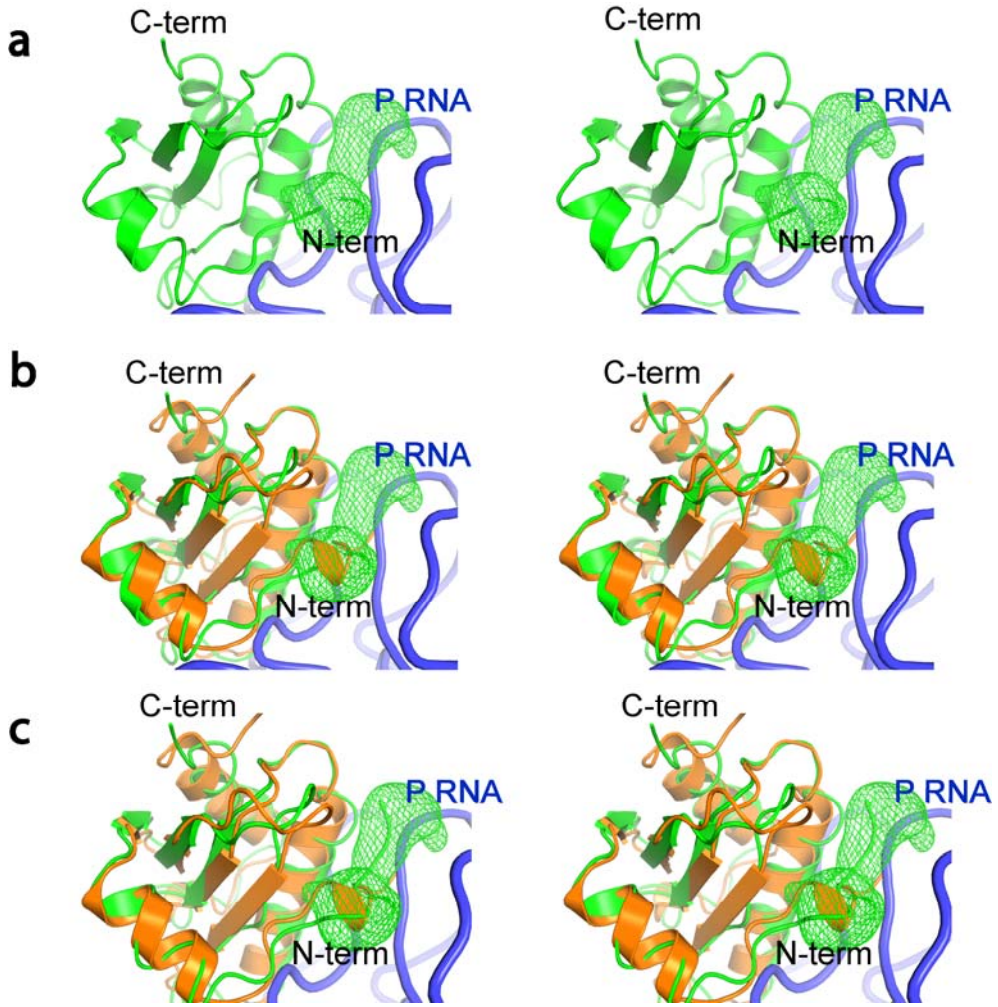

Figure S10 | Structural refinement reveals the position of the N-terminus of the *T. maritima* protein. a, Stereo diagram of the RNase P complex built using the original *T. maritima* RNase P protein structure (1NZ0)[1616] (green) which includes only amino acids 9 – 117. After several refinement cycles, unaccounted for electron density near the N-terminus shows the position of some of the missing amino acids. The diagram shows positive electron density in a difference Fourier map (green mesh, SigmaA weighted (Fo-Fc) map calculated with Buster[6] contoured at +3.75 rmsd) and the model for the complex. **b**, Stereo diagram showing a superposition of the RNase P *B. subtilis* protein (orange) (PDB: 1A6F)[20] on the *T. maritima* protein (green) in the complex. The two proteins are very similar in structure despite belonging to different RNase P types. The superposition shows that the N-terminus residues in the *B. subtilis* protein coincide with the positive density in the Fo-Fc map (green mesh, SigmaA weighted (Fo-Fc) map calculated with Buster[6] contoured at +3.75 rmsd). The *B. subtilis* protein served as a guide to build the N-terminus of the

T. maritima protein in the complex and to confirm the overall position and orientation of the protein backbone. **c**, Stereo diagram showing a superposition of the *B. subtilis* and *T. maritima* RNase P proteins (orange and green, respectively) after model building the N-terminus of the protein in the complex. In all panels, only the backbone trace of the P RNA (blue) is shown.

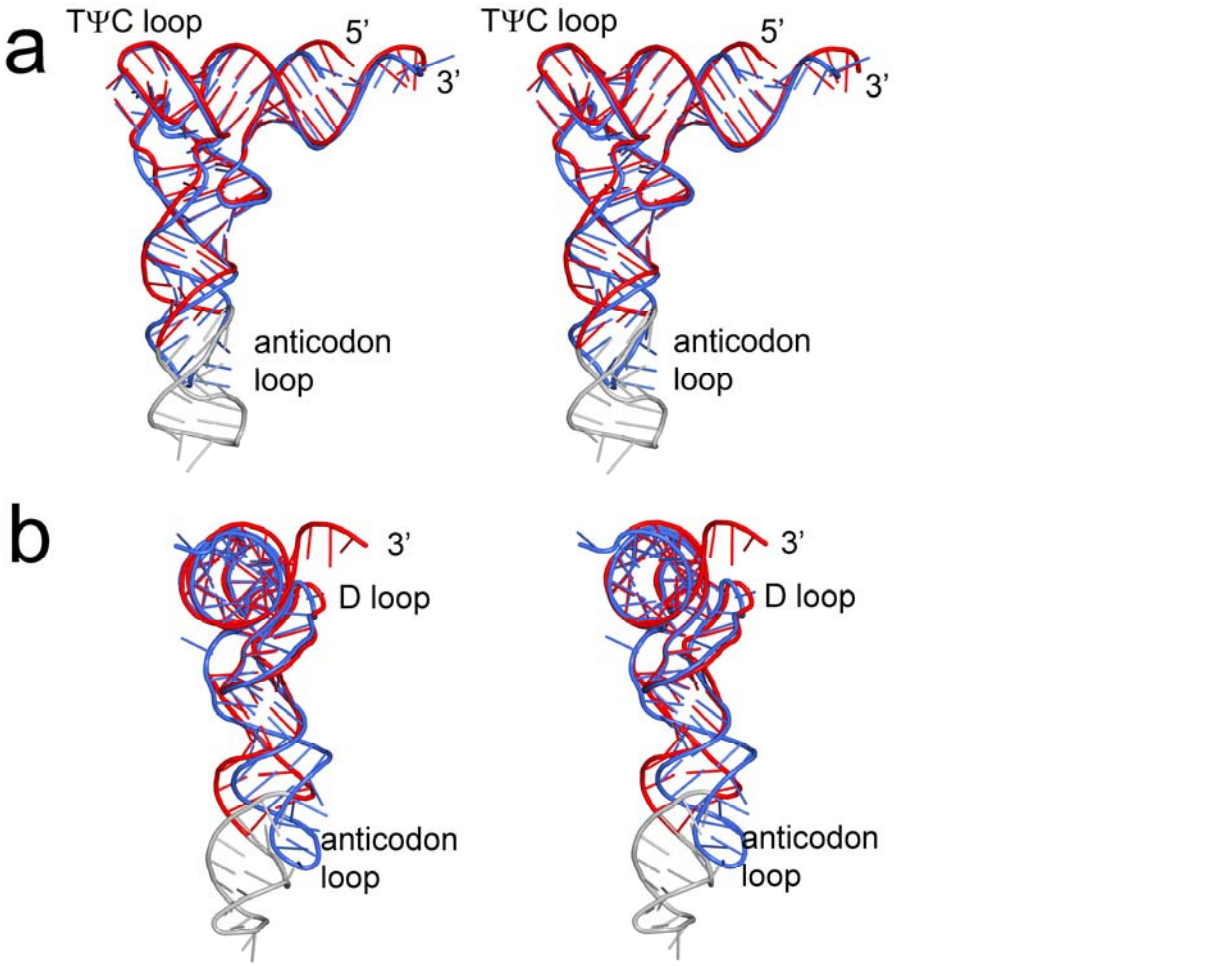

Figure S11 | Superposition of free tRNA and tRNA in the holenzyme/tRNA complex. a, Stereo diagram showing the superposition of yeast $tRNA^{phe}$ (ref. 21)(PDB ID: 1EHZ) (blue) on the tRNA in the RNase P holoenzyme/tRNA complex (red). Sugar phosphate backbone atoms were used in the superposition (normalized rmsd ~1.6 Å). **b,** Stereo diagram showing the superposition of the acceptor stem of yeast $tRNA^{Phe}$ (blue) on the acceptor stem of tRNA in the RNase P holoenzyme/tRNA complex (red). The normalized rmsd for the sugar phosphate backbone atoms in the acceptor stems is 0.8 Å. The diagram shows that the acceptor stem remains largely unchanged, but there is a small movement of the anticodon stem with respect to the acceptor stem. In both diagrams, the additional

nucleotides added to promote crystal formation are shown in grey. **c,** Sequence comparison between the yeast $tRNA^{Phe}$ (blue) and *T. maritima* $tRNA^{Phe}$. The two tRNA sequences are approximately 63% identical.

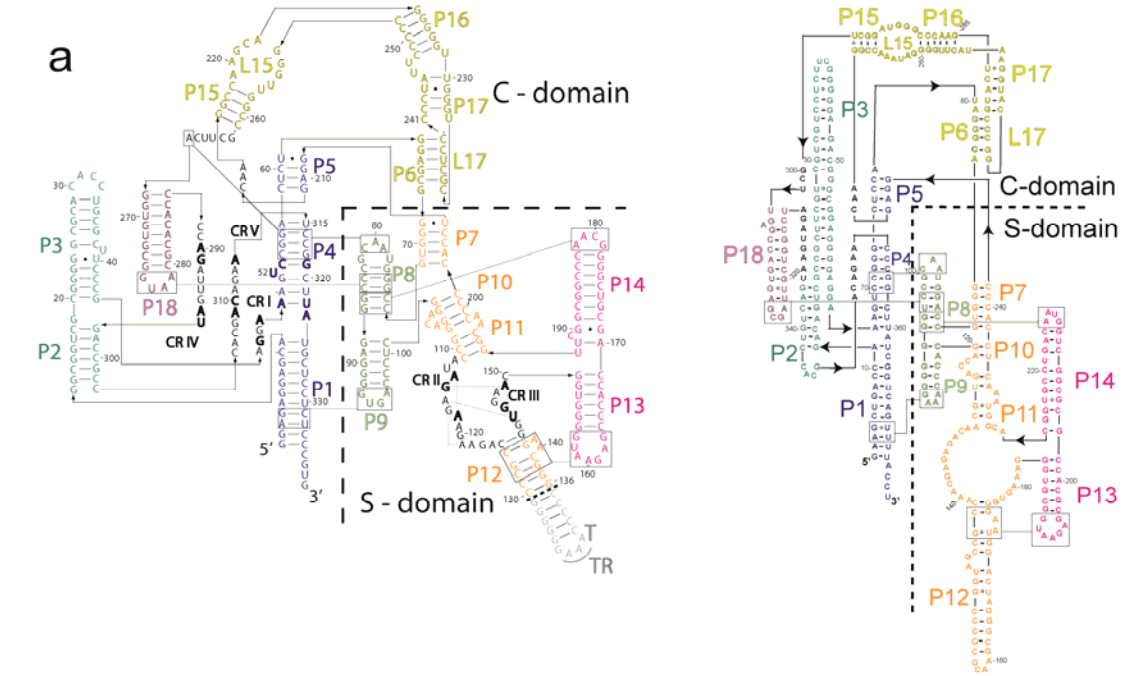
a
C - domain
S - domain
P1
P2
P3
P4
P5
P6
P7
P8
P9
P10
P11
P12
P13
P14
P15
P16
P17
P18
L15
L17
CR I
CR II
CR III
CR IV
CR V
T
TR
5′
3′
C-domain
S-domain

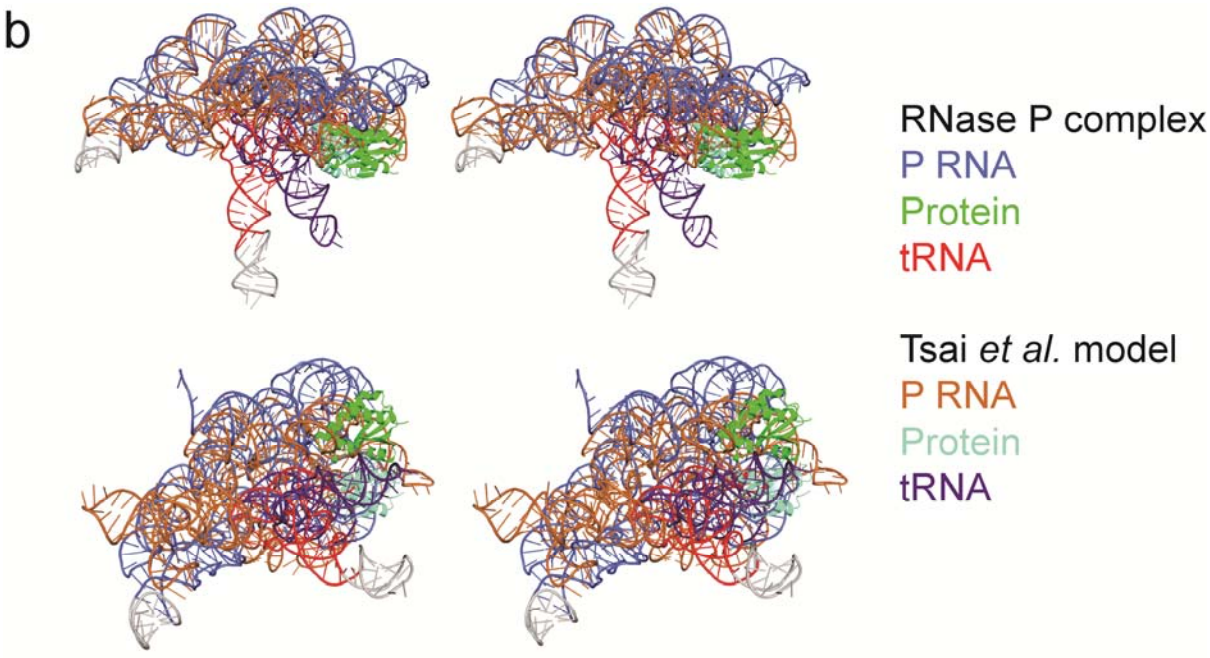
b
RNase P complex
P RNA
Protein
tRNA
Tsai *et al.* model
P RNA
Protein
tRNA

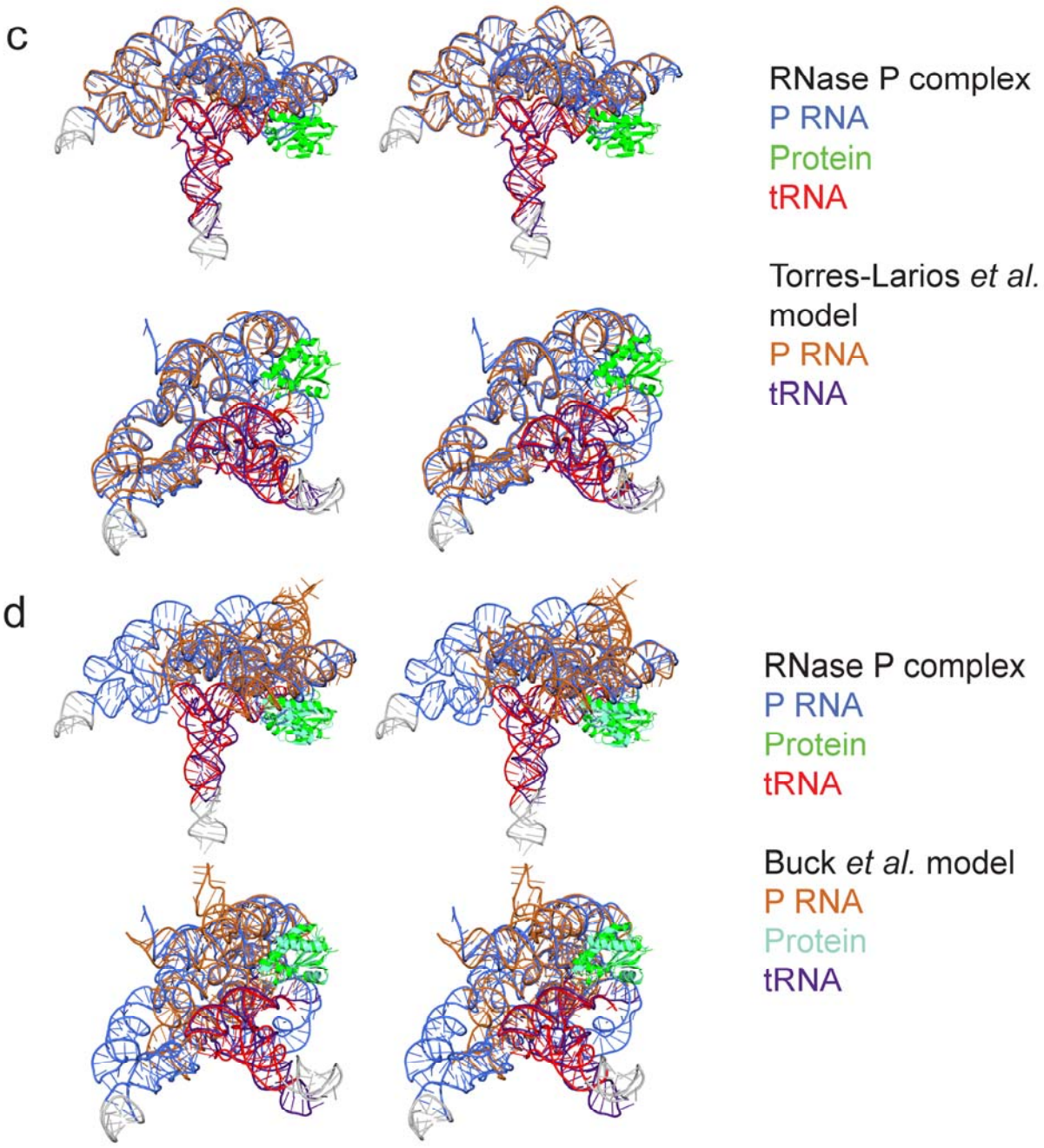

Figure S12 | Comparison of the RNase P holoenzyme/tRNA complex and models of the complex. a, Comparison of the secondary structure diagram obtained from the holenzyme/tRNA complex (left) and a secondary structure diagram derived from the model proposed by Massire *et al*.[22,23] (right). Note the overall excellent agreement in the definition of the paired regions and the general arrangement of the secondary structure elements. For ease of comparison, the diagram obtained from the molecular model[31] has been rotated by 180° and the secondary structure elements are colored identically in both diagrams and following

the same scheme as in Figure S1. **b,** Comparison with the holoenzyme/tRNA molecular model of Tsai *et al.*[24]. The local agreement between the two structures is good, but the overall structure of the holenzyme/tRNA complex model is different. It should be noted that this model was generated and proposed prior to the availability of any experimental structural information on any large region of the P RNA. The model places the tRNA and the protein on the same face of the P RNA as in the complex structure and with a similar overall orientation. For the comparison, the two P RNA structures were aligned by matching only phosphate backbone atoms in the helical regions (total number of atoms matched: 1412). All helical regions were included in the alignment. The normalized rmsd[18] between the two models is 10.7 Å. **c,** Comparison with a P RNA/tRNA model[25] built based on the structure of the *T. maritima* P RNA molecule[19]. The model was built guided only by known interactions between the S-domain of RNase P and tRNA. The model places the tRNA in the correct position and orientation, but the model did not help in identifying interactions with the 5' and 3' end of the tRNA molecule or in locating precisely the active site. The normalized rmsd between the two P RNA structures is 1.4 Å for 1821 atoms matched. **d,** Comparison with the holoenzyme/tRNA model of Buck *et al.*[26] built based on the structure of the *B. stearothermophilus* P RNA[15] and chemical footprinting data[27]. The model agrees well with the structure of the holenzyme/tRNA complex in the general arrangement of the three components and places them in the correct general relative position. The S-domain structure is missing in the model resulting in no tRNA/S-domains interactions and the active site was assigned to be at a different location. The normalized rmsd between the two catalytic domains of the P RNA structures is 1.4 Å for 968 atoms matched. In all comparisons the P RNA, protein, and tRNA from the structure of the complex are colored blue, green and red, identically to Figure 1. The P RNA, protein and tRNA from the models are colored orange, cyan and purple respectively. Superpositions were done with the program lsqman[18].

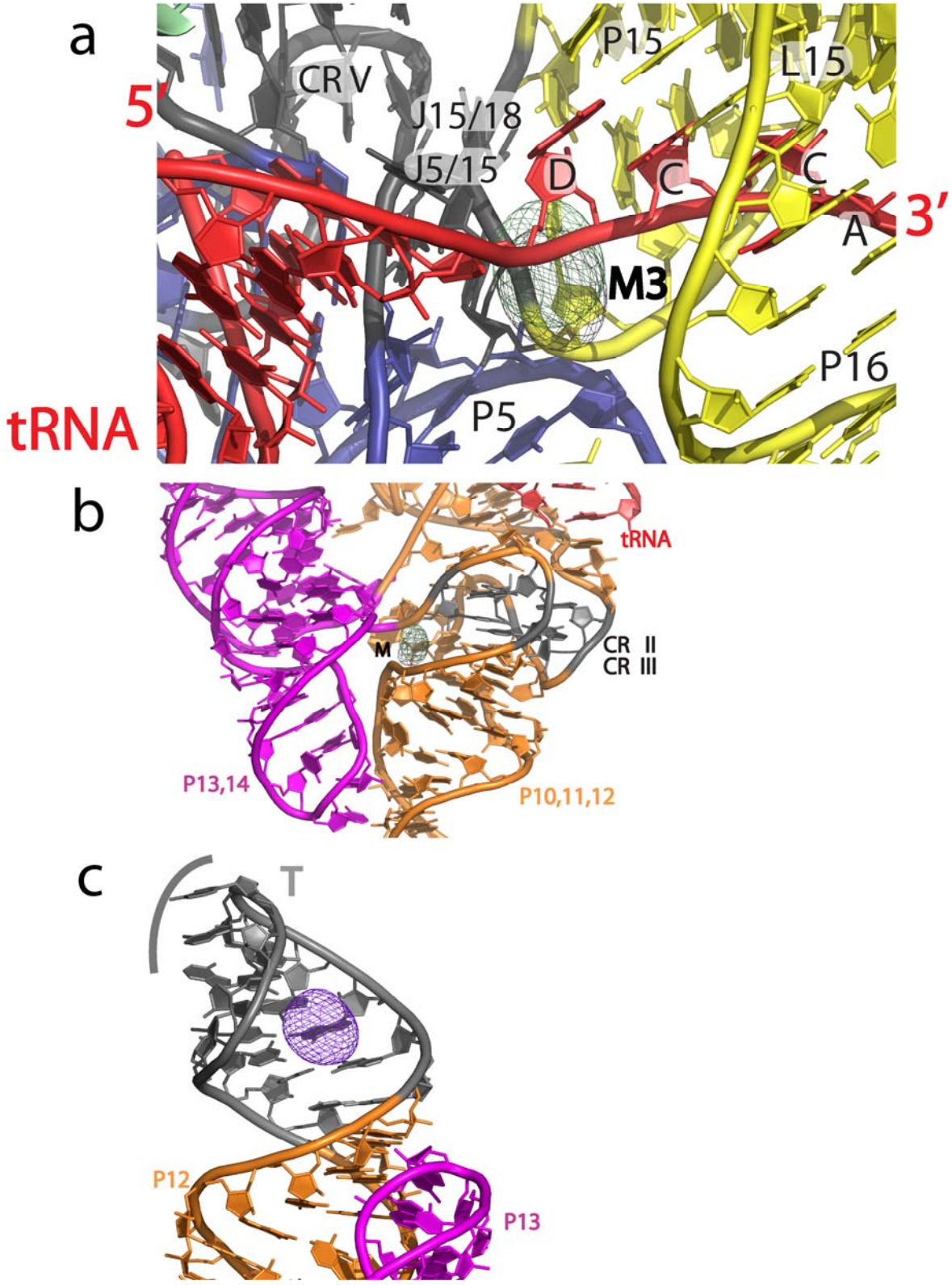
a
5′
CR V
J15/18
J5/15
P15
L15
D
C
C
A
3′
M3
P16
P5
tRNA
b
tRNA
M
CR II
CR III
P13,14
P10,11,12
c
T
P12
P13

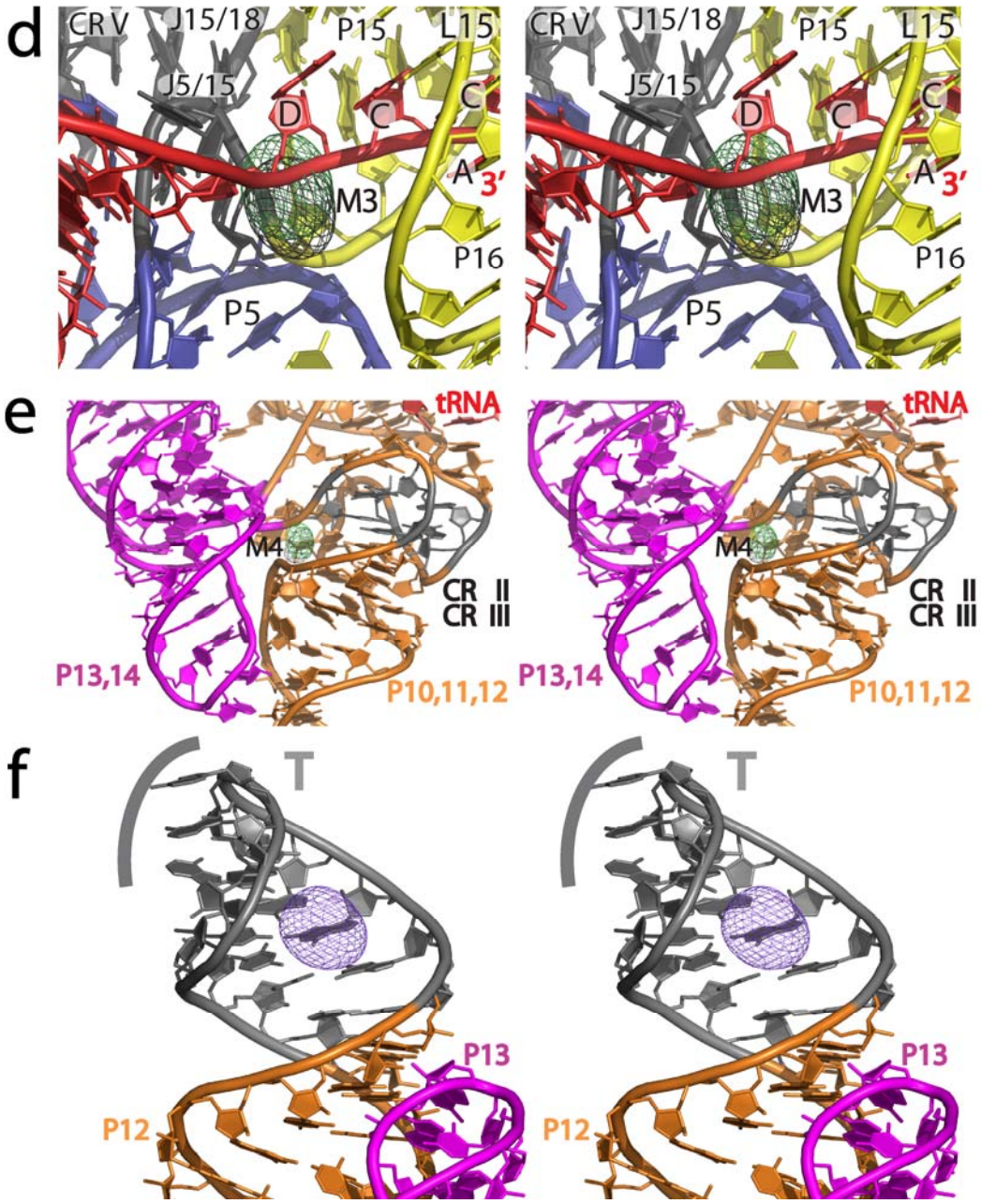

Figure S13 | Identification of structural metal sites critical for RNase P function and structure determination. a, Metal ion (M3) at the tRNA 3′ CCA binding region. To locate high affinity metal binding sites, crystals were soaked in different lanthanides. Sm^{3+} (black) and Eu^{3+} (green) anomalous difference maps contoured at 8.0 rmsd reveal both M3-P RNA (A214 and G215 phosphate oxygen) and M3-tRNA (A73 and C74 phosphate oxygen) contacts. The M3 metal ion binding site is adjacent to the 3′ CCA and helps to stabilize intermolecular base pairing and the RNase P active site environment. **b,** A metal ion (M4) located at the interface of J12/13, the P13 loop, and the P12 internal adenosine bulge stabilizes the

universally conserved T-loop region (CR-II and CR-III, shown in grey) that is required for substrate recognition. Sm^{3+} (black) and Eu^{3+} (green) anomalous difference maps are contoured at the 8.0 rmsd level. **c,** Iridium hexamine binds at an engineered G-U metal site adjacent to the tetraloop-tetraloop receptor tertiary RNA module ((T)-tetraloop receptor (TR) RNA module (light grey)). The iridium hexamine anomalous difference map (purple) is contoured at 8.0 rmsd level. Panels **d**, **e**, and **f** correspond to stereo diagrams of panels **a**, **b**, and **c**, respectively.

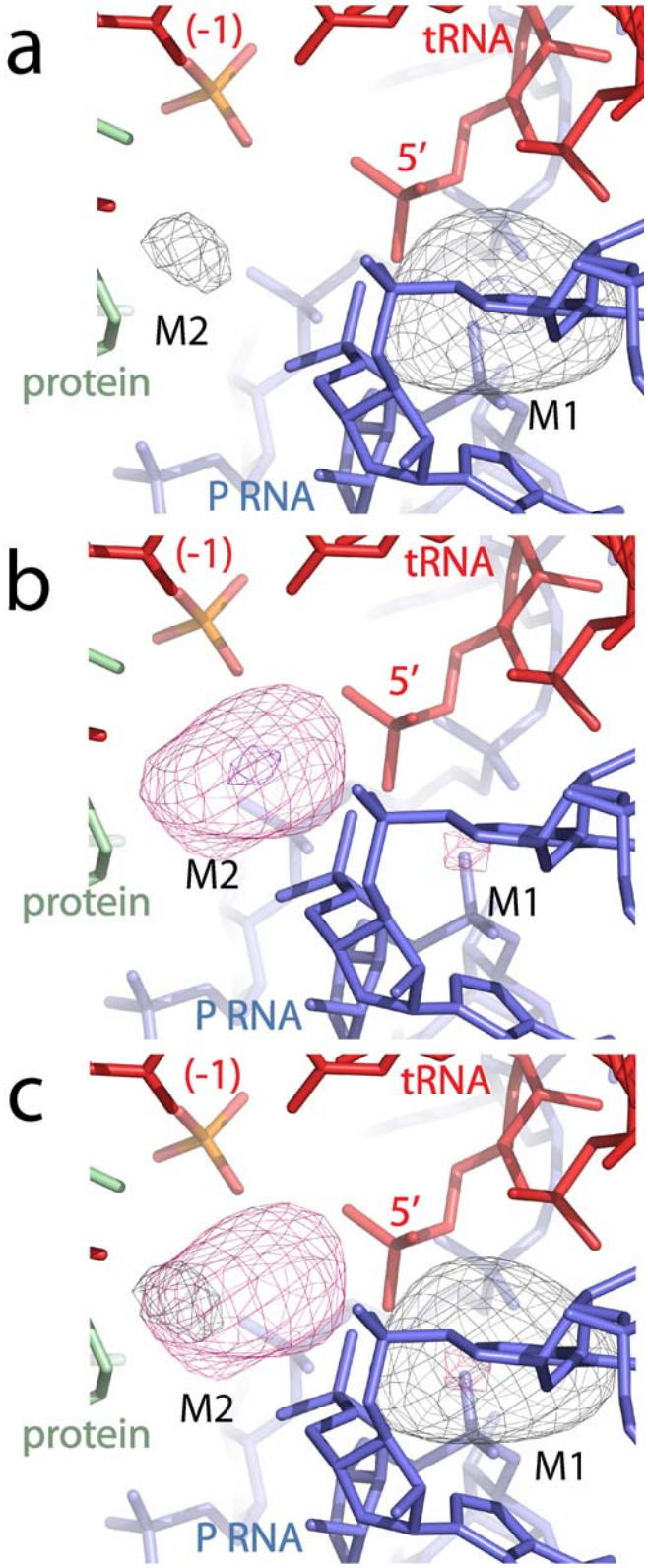
a
(-1)
tRNA
5′
M2
protein
M1
P RNA
b
(-1)
tRNA
5′
M2
protein
M1
P RNA
c
(-1)
tRNA
5′
M2
protein
M1
P RNA

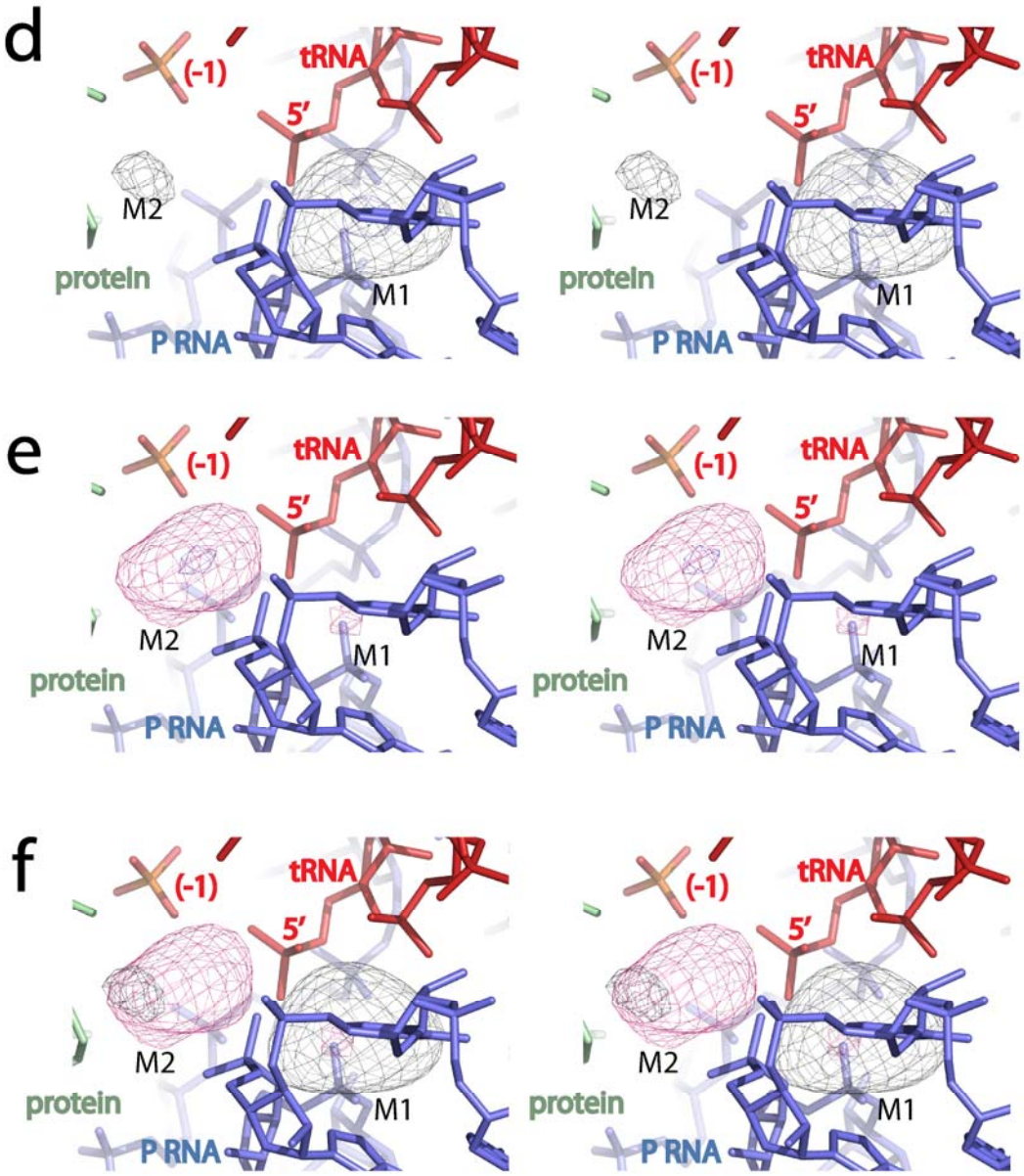

Figure S14 | Identification of two metal ions at the RNase P active site. Difference Fourier ($(F_o-F_c)\exp(i\phi_{calc})$) electron density maps were used to verify the metal positions. Phases from the final, refined model after several cycles of refinement without the active site metals were used. **a,** For crystals soaked with just Sm^{3+}, density contoured at the 4.2 rmsd level (grey) shows both M1 and M2 sites, but only the M1 site is occupied at the 9.5 rmsd level (blue). **b,** For crystals soaked in the presence of a 7 nucleotide leader RNA and Sm^{3+}, density contoured the 4.2 rmsd level (magenta) shows both the M1 and M2 sites, but only the M2 site is occupied at the 6.5 rmsd level (purple). **c,** Superposition of F_o-F_c maps from A (grey) and B (magenta). Both maps are contoured at the 4.2 rmsd level Sm^{3+} and Eu^{3+}

anomalous difference maps further confirmed M1 and M2 metal ion locations (data not shown). The high concentration of monovalent ions (Li^{1+}) in the crystals indicate that these lanthanide binding sites correspond to highly specific sites, as suggested by studies of divalent metal ion binding in high monovalent milieus[28]. Panels **d**, **e**, and **f** represent stereo diagrams of panels **a**, **b**, and **c**, respectively.

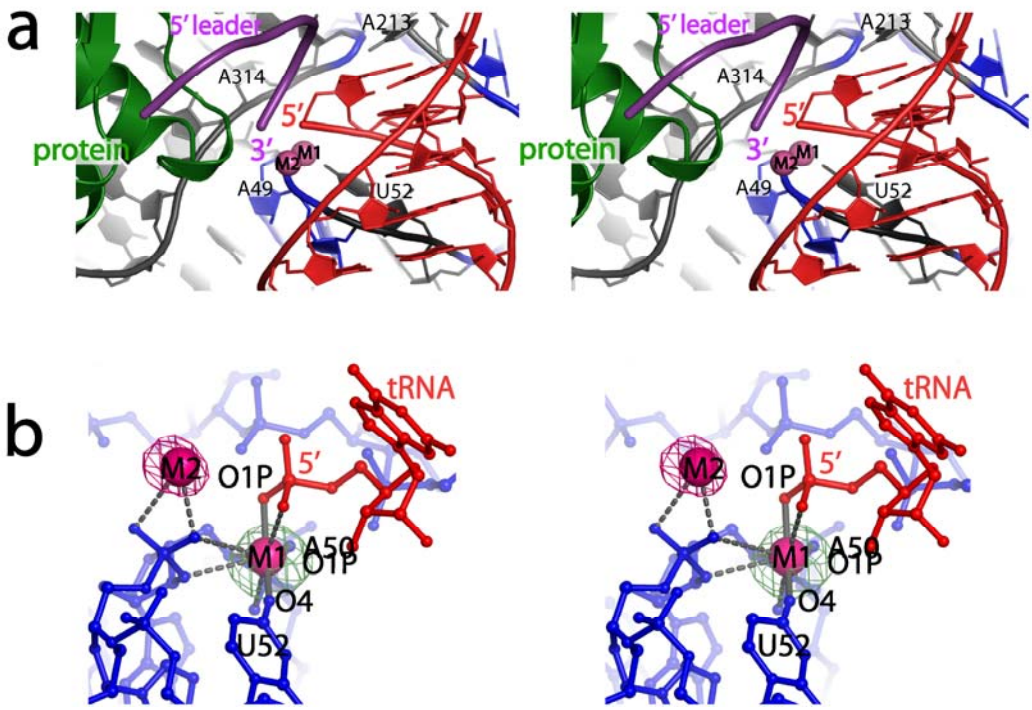

Figure S15 | Stereo diagram of the RNase P active site environment. Supplemental to Figure 5. a, Stereo diagram showing the position of the mature tRNA (red), the leader (purple), the protein component (green), and the P RNA (blue and grey) at the enzyme active site. **b,** Stereo diagram showing two metal ions at the RNase P active site. The stereo diagram shows isomorphous differences electron density maps ($(F_{HA}-F_{calc})\exp(i\phi_{calc})$) for Eu^{3+} (green mesh) and Sm^{3+} (with 5′ leader, pink mesh) soaks overlaid on the model for the active site, contoured at 9.5 and 5.5 rmsd levels, respectively. Metal ions (M1 and M2) are ≤ 4 Å of the 5′ phosphate of mature tRNA. The M1-M2 metal-metal distance is ~4.9 Å and contains a possible bridging oxygen ligand (G51 O2P). As the structure represents a product/ribozyme complex, this long metal-metal distance is not surprising as the leader has separated from the mature tRNA carrying the second metal with it. The M1 metal has inner-sphere contacts (≤ 2.1 Å, solid grey bonds) with both tRNA (G1 O1P) and the P RNA (A50 O1P and U52 O4) oxygens. Other possible ligands within 3.5 Å of M1 or M2 are represented by dashed grey lines (Table STIV).

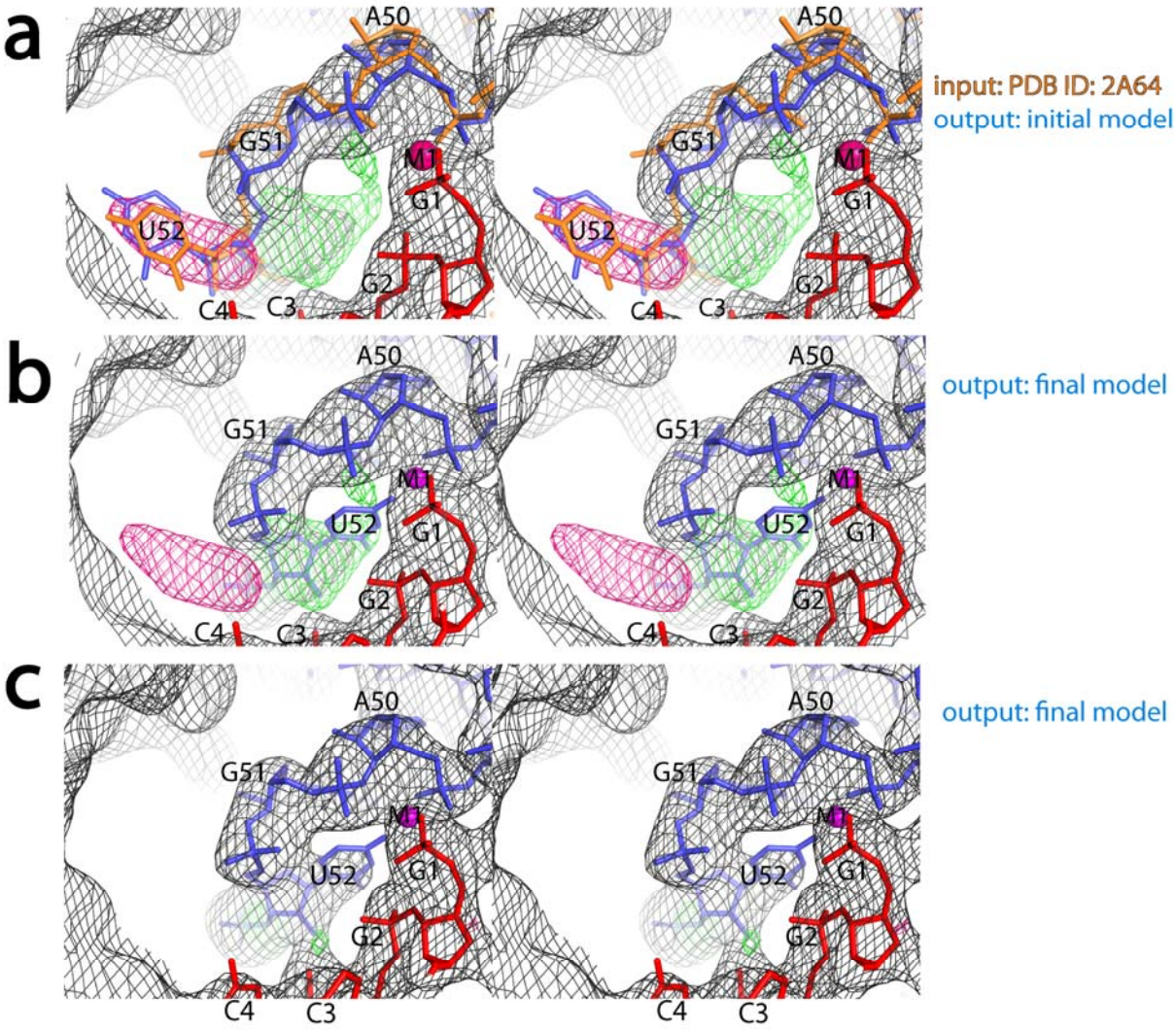

Figure S16 | Example of model building in the vicinity of the RNase P active site. The figure serves to illustrate the model building process using a low resolution electron density map. The experimental electron density map and previous P RNA apo-structures (PDB 2A64 and 2A2E)[15,19] were used to build the entire P RNA structure. In some regions, such as the active site region shown here, the models were either incomplete (2A2E) or show a different conformation (2A64) from the one in the final model. During the initial model building and also during the refinement process it was possible to observe differences in conformation and correct errors in the model. **a,** Stereo diagram of a model with the conserved U52 base placed in an extrahelical position as seen in the structure of *B. stearothermophilus*[15]. The P4 helix from the original *B. stearothermophilus* apo-structure (orange, PDB 2A64) was placed into the experimental map and the model extensively refined using BUSTER[6]. The resulting refined model (blue P RNA) and difference maps maps

(SigmaA weighted (F_o-F_c), ϕ_{calc}) show that U52 is not correctly positioned. The U52 nucleotide is in negative density (-3.75 rmsd, magenta), indicative of an incorrect placing. Positive density (+3.75 rmsd, green), representing unaccounted for electron density, shows the correct position of the nucleotide. For guidance, the corresponding output $2F_o$-F_c map (1.5 rmsd, SigmaA weighted ($2F_o$-F_c), ϕ_{calc}) is shown in black. **b,** Stereo diagram of the final structural model (blue P RNA) of the RNase P complex. The SigmaA weighted $2F_o$-F_c and F_o-F_c maps from **(a)** are shown to illustrate how the U52 nucleotide now clearly fits into the maps. **c,** Stereo diagram of the final structural model (blue P RNA), showing the final SigmaA weighted $2F_o$-F_c map (contoured at 1.5 rmsd). In addition, the final SigmaA weighted F_o-F_c maps is also shown (green: +3.75 rmsd and magenta: -3.75 rmsd. There is almost no residual density in the SigmaA weighted F_o-F_c map, indicating that nucleotides are now correctly positioned. In all diagrams **(a-c)**, the tRNA is shown as red sticks and the M1 metal is represented as a magenta sphere.

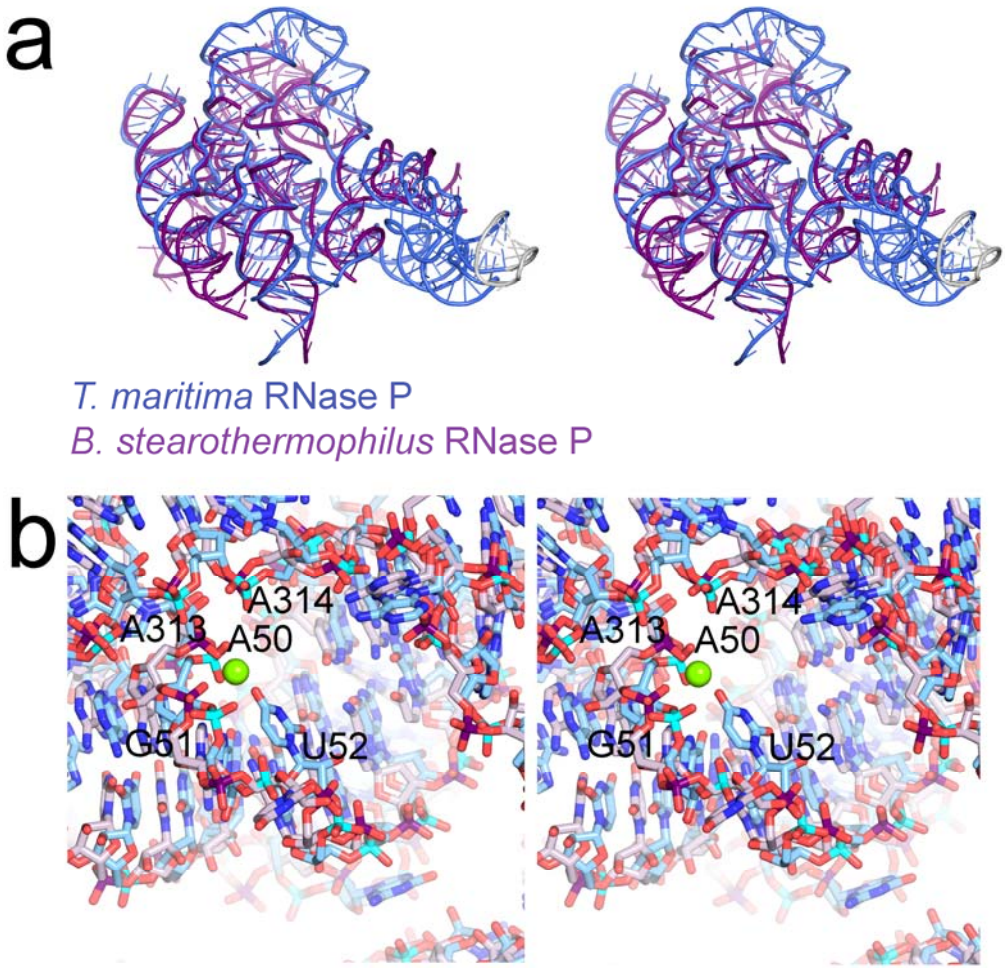

Figure S17 | Superposition of *B. stearothermophilus* P RNA and *T. maritima* P RNA from the holenzyme/tRNA complex. a, Stereo diagram showing the superposition of the entire catalytic domain and parts of the specificity domain of *B. stearothermophilus* P RNA (purple) and the *T. maritima* P RNA in the holoenzyme/tRNA complex (blue). The normalized rms deviation for the common phosphate backbone atoms in the catalytic domain is 1.4 Å (ref. 18). The *B. stearothermophilus* specificity domain was not included in the superposition as only a small region is present in the crystal. **b,** Stereo diagram showing a superposition of the active site region in the two molecules. For clarity, the carbon and phosphorous atoms in *B. stearothermophilus* P RNA are shown in light purple and purple, respectively, and in light blue and cyan in the *T. maritima* P RNA structure. Magnesium ions in the *T. maritima* structure are shown in green. The diagram illustrates the similarity in the active site for the type A and B RNase P molecules. The active site metal adjacent to U52 appears to have an equivalent in the *B.*

stearothermophilus structure, where a metal site (termed the M6 site) is reported to be in the vicinity of U50 and A390[29], but coordinates for the metal site were not available for direct comparison. The universally conserved U52 nucleotide that contacts a metal in the complex structure is in a different position in the *B. stearothermophilus* structure as it is involved in crystallographic contacts. It is likely that the catalytic metal M1 is present in the apo-structure as well, although not in the exact position as the tRNA ligands are absent. Given that the active site includes many nucleotides from universally conserved regions, it is expected that the active site in RNase P from all organisms will be very similar.

References

1 Strong, M. *et al.* Toward the structural genomics of complexes: crystal structure of a PE/PPE protein complex from Mycobacterium tuberculosis. *Proc Natl Acad Sci U S A* **103**, 8060-8065 (2006).

2 Diederichs, K. & Karplus, P. A. Improved R-factors for diffraction data analysis in macromolecular crystallography. *Nat. Struct. Biol.* **4**, 269-275 (1997).

3 Collaborative Computational Project 4. The CCP4 suite: programs for protein crystallography. *Acta Crystallogr.* **D50**, 760-763 (1994).

4 Fortelle, E. & Bricogne, G. Maximum-Likelihood Heavy-Atom Parameter Refinement for Multiple Isomorphous Replacement and Multiwavelength Anomalous Diffraction Methods. *Meth. Enzymol.* **276**, 472-494 (1997).

5 Murshudov, G. N., Vagin, A. A. & Dodson, E. J. Refinement of macromolecular structures by the maximum-likelihood method. *Acta Crystallogr.* **D53**, 240-255 (1997).

6 Blanc, E. *et al.* Refinement of severely incomplete structures with maximum likelihood in BUSTER-TNT. *Acta Crystallogr D Biol Crystallogr* **60**, 2210-2221 (2004).

7 Brunger, A. T. The free R value: a novel statistical quantity for assessing the accuracy of crystal structure. *Nature* **355**, 472-474 (1992).

8 Krasilnikov, A. S. & Mondragón, A. On the occurrence of the T-loop RNA folding motif in large RNA molecules. *RNA* **9**, 640-643 (2003).

9 Tallsjo, A., Kufel, J. & Kirsebom, L. A. Interaction between Escherichia coli RNase P RNA and the discriminator base results in slow product release. *RNA* **2**, 299-307 (1996).

10 Tallsjo, A., Svard, S. G., Kufel, J. & Kirsebom, L. A. A novel tertiary interaction in M1 RNA, the catalytic subunit of Escherichia coli RNase P. *Nucleic Acids Research* **21**, 3927-3933 (1993).

11 Hsieh, J., Walker, S. C., Fierke, C. A. & Engelke, D. R. Pre-tRNA turnover catalyzed by the yeast nuclear RNase P holoenzyme is limited by product release. *RNA* **15**, 224-234 (2009).

12 Reich, C., Olsen, G. J., Pace, B. & Pace, N. R. Role of the protein moiety of ribonuclease P, a ribonucleoprotein enzyme. *Science* **239**, 178-181 (1988).

13 Tallsjo, A. & Kirsebom, L. A. Product release is a rate-limiting step during cleavage by the catalytic RNA subunit of Escherichia coli RNase P. *Nucleic Acids Res* **21**, 51-57 (1993).
14 Hartmann, R. K., Gossringer, M., Spath, B., Fischer, S. & Marchfelder, A. The making of tRNAs and more - RNase P and tRNase Z. *Prog Mol Biol Transl Sci* **85**, 319-368 (2009).
15 Kazantsev, A. V. *et al.* Crystal structure of a bacterial ribonuclease P RNA. *Proc. Natl. Acad. Sci. U. S. A.* **102**, 13392-13397 (2005).
16 Kazantsev, A. V. *et al.* High-resolution structure of RNase P protein from Thermotoga maritima. *Proc Natl Acad Sci U S A* **100**, 7497-7502 (2003).
17 Landau, M. *et al.* ConSurf 2005: the projection of evolutionary conservation scores of residues on protein structures. *Nucleic Acids Res* **33**, W299-302 (2005).
18 Kleywegt, G. J. Use of non-crystallographic symmetry in protein structure refinement. *Acta Crystallogr D Biol Crystallogr* **52**, 842-857 (1996).
19 Torres-Larios, A., Swinger, K. K., Krasilnikov, A. S., Pan, T. & Mondragón, A. Crystal structure of the RNA component of bacterial ribonuclease P. *Nature* **437**, 584-587 (2005).
20 Stams, T., Niranjanakumari, S., Fierke, C. A. & Christianson, D. W. Ribonuclease P protein structure: evolutionary origins in the translational apparatus. *Science* **280**, 752-755 (1998).
21 Shi, H. & Moore, P. B. The crystal structure of yeast phenylalanine tRNA at 1.93 A resolution: a classic structure revisited. *RNA* **6**, 1091-1105 (2000).
22 Masquida, B., Jossinet, F. & Westhof, E. in *Ribonuclease P* Vol. 10 *Protein Reviews* (eds F. Liu & S. Altman) Ch. 3, 41-62 (Springer Science+Business Media, LLC, 2010).
23 Massire, C., Jaeger, L. & Westhof, E. Derivation of the three-dimensional architecture of bacterial ribonuclease P RNAs from comparative sequence analysis. *J. Mol. Biol.* **279**, 773-793 (1998).
24 Tsai, H. Y., Masquida, B., Biswas, R., Westhof, E. & Gopalan, V. Molecular modeling of the three-dimensional structure of the bacterial RNase P holoenzyme. *J. Mol. Biol.* **325**, 661-675 (2003).
25 Torres-Larios, A., Swinger, K. K., Pan, T. & Mondragón, A. Structure of ribonuclease P--a universal ribozyme. *Curr Opin Struct Biol* **16**, 327-335 (2006).
26 Buck, A. H., Kazantsev, A. V., Dalby, A. B. & Pace, N. R. Structural perspective on the activation of RNase P RNA by protein. *Nat. Struct. Mol. Biol.* (2005).
27 Buck, A. H., Dalby, A. B., Poole, A. W., Kazantsev, A. V. & Pace, N. R. Protein activation of a ribozyme: the role of bacterial RNase P protein. *EMBO J.* **24**, 3360-3368 (2005).
28 Bukhman, Y. V. & Draper, D. E. Affinities and selectivities of divalent cation binding sites within an RNA tertiary structure. *J Mol Biol* **273**, 1020-1031 (1997).
29 Kazantsev, A. V., Krivenko, A. A. & Pace, N. R. Mapping metal-binding sites in the catalytic domain of bacterial RNase P RNA. *RNA* **15**, 266-276 (2009).